NASA TN D-996

TECHNICAL NOTE

D-996

AN ANALYTICAL TREND STUDY OF PROPELLER WHIRL INSTABILITY

By John L. Sewall

Langley Research Center
Langley Station, Hampton, Va.

NATIONAL AERONAUTICS AND SPACE ADMINISTRATION
WASHINGTON April 1962

N62-12917

ERRATA

NASA Technical Note D-996

By John L. Sewall
April 1962

Page 10: Errors in equations (8b) and (8c) require that these equations be corrected as follows:

$$A_1 = \frac{1}{\mu}\frac{\Omega}{\omega_\theta}\frac{J}{\pi}\left\{-\frac{\Omega}{\omega_\theta}\frac{J}{\pi}C_{Y_\psi}\left(1+\frac{e_\psi}{e}\frac{I_Y}{I_Z'}\right)-\frac{D}{e}\left(2\zeta_\psi\frac{\omega_\psi}{\omega_\theta}P_1+2\zeta_\theta\frac{I_Y}{I_Z'}P_1'\right)\right.$$
$$\left.+\frac{1}{\mu}\frac{\Omega}{\omega_\theta}\frac{J}{\pi}\left(\frac{D}{e}\right)^2\frac{I_Y}{I_Z'}P_1P_1'+2\frac{I_Y}{I_Z'}\left[\frac{I_X\Omega}{I_Y\omega_\theta}\left(P_3+P_3'\right)+\frac{2}{\mu}\frac{\Omega}{\omega_\theta}\frac{J}{\pi}P_3P_3'\right]\right\} \quad (8b)$$

$$A_0 = \frac{1}{\mu}\left(\frac{\Omega}{\omega_\theta}\frac{J}{\pi}\right)^2\left[-C_{Y_\psi}\left(\frac{\omega_\psi^2}{\omega_\theta^2}+\frac{e_\psi}{e}\frac{I_Y}{I_Z'}\right)+\frac{1}{\mu}\left(\frac{\Omega}{\omega_\theta}\frac{J}{\pi}\right)^2\frac{I_Y}{I_Z'}\left(C_{Y_\psi}{}^2\frac{e_\psi}{e}+\frac{D^2}{e^2}P_2P_2'\right)\right] \quad (8c)$$

Page 13: In the definition of $P_D{}^2$ at the top of page 13 the term within the second parentheses is incorrect. The correct definition is

$$P_D{}^2 = \kappa\left(\frac{\Omega}{\omega_\theta}\frac{J_D}{\pi}\right)^2 = \kappa\left(\frac{V_D}{\frac{D}{2}\omega_\theta}\right)^2$$

NASA-Langley, 1962

Issued 9-28-62

NATIONAL AERONAUTICS AND SPACE ADMINISTRATION

TECHNICAL NOTE D-996

AN ANALYTICAL TREND STUDY OF PROPELLER WHIRL INSTABILITY

By John L. Sewall

SUMMARY

This paper reports the results of an analytical trend study that extends the work done by Reed and Bland in NASA Technical Note D-659 and Houbolt and Reed in Institute Aerospace Science Paper No. 61-34 on the precessional instability of a simulated engine-propeller configuration. Primary attention is given to the applications of simplified linear equations which are derived and which define the borderline conditions between stable and unstable motion in terms of damping coefficients in pitch and yaw. The equations as derived apply to the case of separate elastic centers in pitch and yaw, and the results of some studies are included to show the effects of separate elastic centers. For the case of the common elastic center, the paper confirms the results reported in the two papers mentioned previously as to stiffness, damping, elastic-center location, and mass- or inertia-density ratio over a broader range of these parameters than was previously considered. The present study also includes the effects of polar-to-pitch (or polar-to-yaw) moment-of-inertia ratio and the effects of aerodynamic forces on whirl frequency at extreme values of yaw-to-pitch frequency ratio. The occurrence of engine-propeller divergence at speeds less than the critical whirl speed is shown to be unlikely unless the system becomes very weak in one direction (that is, pitch or yaw) relative to the other. The effects of the significant whirl parameters are shown in various figures which summarize the analytical trends.

INTRODUCTION

For most piston engines presently in service, vibrations due to engine operation are isolated, insofar as possible, by sets of spring-mountings equally spaced in a ring encircling the engine in the manner recommended by Taylor and Browne in reference 1. In analyzing the dynamics of this system, these writers recognized that an instability could occur due to the interaction between gyroscopic and aerodynamic forces and moments acting on the engine-propeller configuration with the propeller spinning. This instability, which has come to be known as propeller whirl, is characterized by a wobbling motion of the propeller shaft with the propeller hub describing, in general, an elliptical path.

Power plants with spring-mounting systems similar to that described in reference 1 have apparently had sufficient margins in spring stiffness and damping to be free of this whirl instability within their respective ranges of operation. Consequently, propeller whirl has not been regarded as a particularly critical aircraft dynamics problem.

However, with the introduction of radically different engine mountings, increased engine-power-to-engine-weight ratio, increased vibration isolation requirements, and with the continued use of long overhung nacelles, this instability is once again of interest for such propeller-driven aircraft. Recent work on the problem is reported in references 2 and 3 which deal with simplified representations of the engine-propeller system and provide an understanding of the basic nature of the problem. Effects of the wing are not included, and the motion is described by two degrees of freedom in pitch and yaw with aerodynamic forces and moments based either on the propeller coefficients of Ribner (ref. 4) or on the coefficients derived in reference 3. Both references 2 and 3 are mainly concerned with solutions of the stability equation defining the borderline conditions between damped and undamped motions but also give attention to the transient response of the system obtained by solutions of the equations of motion on an analog computer.

The purpose of the present paper is to report an analytical trend study covering the ranges of dimensionless parameters listed in table I, which extends the ranges covered in references 2 and 3. The same idealized representation as that of reference 2 is considered, although the solution of the stability equation is presented in somewhat different form, and provision is made for separate elastic centers in pitch and yaw. Some calculations were made to show the effects of separate elastic centers, but except for these cases, all the analytical trends presented are based on a common elastic center as was done in references 2 and 3. Damping in the structure is represented as viscous damping, and linear relations between this type of damping and total damping are derived from the stability equation. These linear relations are used to show the effects of such dimensionless parameters as yaw-to-pitch frequency ratio, inertia-density ratio, and advance ratio. Consideration is also given, as in reference 3, to the static aeroelastic phenomenon of divergence for this idealized engine-propeller combination.

SYMBOLS

$a_1 \ldots a_4$, $b_1 \ldots b_4$ coefficients of differential equations of motion, defined by equation (1)

b blade width, ft (See fig. 5.)

A_1, A_0	aerodynamic and damping contributions to whirl frequency (eq. (8a)), defined by equations (8b) and (8c)
B_n	total damping coefficient in nth whirl mode, sec^{-1}
$c_0 \ldots c_3$	coefficients of equation (2)
C_{m_ψ}	pitching-moment derivative with respect to yaw
C_{m_q}	pitching-moment derivative with respect to pitching velocity
C_{Y_θ}	side-force derivative with respect to pitch (not actually given in ref. 4; approximated in refs. 2 and 3)
C_{Y_ψ}	side-force derivative with respect to yaw
C_{Y_q}	side-force derivative with respect to pitching velocity
D	propeller diameter, ft
e	moment arm from propeller plane to effective elastic center in pitch, ft
e_ψ	moment arm from propeller plane to effective elastic center in yaw, ft
E	coefficient of divergence equation (eq. (11))
F(s)	quartic stability equation (eq. (2))
f_1	circular propeller whirl frequency in retrograde mode, $\omega_1/2\pi$, cps
f_θ	uncoupled circular frequency in pitch, $\omega_\theta/2\pi$, cps
ζ_ψ, ζ_θ	viscous damping coefficients in yaw and pitch, representing damping in structure and defined by c/c_c where c is usual viscous damping coefficient (proportional to velocity) and c_c is critical damping coefficient
G	coefficient of divergence equation (eq. (11))
I_X	mass polar moment of inertia of propeller about axis of rotation, ft-lb-sec^2

I_Y mass moment of inertia of engine-propeller combination in pitch about elastic center in pitch, ft-lb-sec^2

I_Z' mass moment of inertia of engine-propeller combination in yaw about elastic center in yaw, ft-lb-sec^2

J advance ratio, V/nD

k_θ spring constant of system in pitch, ft-lb/radian

k_ψ spring constant of system in yaw, ft-lb/radian

K_1 intercept of linear equation (7), defined by equation (7b)

K_0 slope of linear equation (7), defined by equation (7a)

K_2, K_3 quantities defined by equations (7c) and (7d)

$P_1, P_2, P_3, \ldots$ aerodynamic quantities defined following equation (7b)

n propeller rotational speed, rps

P_D^2 divergence parameter, see equation (11), $\kappa\left(\frac{\Omega}{\omega_\theta}\frac{J_D}{\pi}\right)^2$

s variable in Laplace transform

V airstream velocity, ft/sec

T_c thrust coefficient, $\frac{\text{Thrust}}{\rho V^2 D^2}$

X, Y, Z coordinate system (see fig. 1)

θ pitch angle, radians

β blade angle, deg (see fig. 5)

κ inertia-density ratio $\frac{\pi\rho D^5/32}{I_Y}$, where numerator is mass moment of inertia of a cylinder of air of length D about propeller axis of rotation

μ inertia-density ratio $\frac{I_Y}{\pi\rho D^4 e/32}$, where the denominator is mass moment of inertia of a cylinder of air of length e about propeller axis of rotation

Ω propeller rotational speed, radians/sec

ω_n frequency of nth precessional mode of propeller shaft (or simply, propeller whirl frequency), radians/sec

ω_θ uncoupled frequency in pitch, $\sqrt{\frac{k_\theta}{I_Y}}$, radians/sec

ρ air density, lb-sec^2/ft^4

ψ yaw angle, radians

ω_ψ uncoupled frequency in yaw, $\sqrt{\frac{k_\psi}{I_Z'}}$, radians/sec

Subscripts:

0 denotes zero lift condition on propeller blade (See fig. 5.)

0.75R denotes property of propeller blade at three-fourths of propeller radius (See fig. 5.)

D divergence

Dots over symbols indicate derivatives with respect to time. Primes denote quantities associated with the elastic center in yaw.

ANALYSIS

Development of Stability Equations

The dynamic behavior of an elastically mounted propeller-engine system in an airstream is represented by a two-degree-of-freedom system in pitch and yaw shown in figure 1. The equations of motion are conveniently written in the form:

$$\ddot{\theta} + a_1\dot{\theta} + a_2\theta + a_3\dot{\psi} - a_4\psi = 0$$

$$\ddot{\psi} + b_1\dot{\psi} + b_2\psi - b_3\dot{\theta} + b_4\theta = 0$$

where the coefficients are defined as follows:

$$
\left.
\begin{aligned}
a_1 &= 2\zeta_\theta\omega_\theta - \frac{\pi\rho D^4 V}{16 I_Y}\left(C_{m_q} - 2\,\frac{e^2}{D^2}\,C_{Y_\psi}\right) \\
a_2 &= \omega_\theta{}^2 - \frac{\pi\rho D^2 e V^2}{8 I_Y}\,C_{Y_\psi} \\
a_3 &= \frac{I_X\Omega}{I_Y} + \frac{\pi\rho D^3 e V}{8 I_Y}\left(\frac{e_\psi}{e}\,C_{m_\psi} + \frac{C_{Y_q}}{2} - \frac{e_\psi}{e}\,\frac{e}{D}\,C_{Y_\theta}\right) \\
a_4 &= \frac{\pi\rho D^3 V^2}{8 I_Y}\left(C_{m_\psi} - \frac{e}{D}\,C_{Y_\theta}\right) \\
b_1 &= 2\zeta_\psi\omega_\psi - \frac{\pi\rho D^4 V}{16 I_Y}\left(\frac{I_Y}{I_Z'}\right)\left(C_{m_q} - 2\,\frac{e_\psi{}^2}{e^2}\,\frac{e^2}{D^2}\,C_{Y_\psi}\right) \\
b_2 &= \omega_\psi{}^2 - \frac{\pi\rho D^2 e V^2 C_{Y_\psi}}{8 I_Y}\left(\frac{e_\psi}{e}\,\frac{I_Y}{I_Z'}\right) \\
b_3 &= \frac{I_Y}{I_Z'}\left[\frac{I_X\Omega}{I_Y} + \frac{\pi\rho D^3 e V}{8 I_Y}\left(C_{m_\psi} + \frac{e_\psi}{e}\,\frac{C_{Y_q}}{2} - \frac{e_\psi}{e}\,\frac{e}{D}\,C_{Y_\theta}\right)\right] \\
b_4 &= \frac{\pi\rho D^3 V^2}{8 I_Y}\left(\frac{I_Y}{I_Z'}\right)\left(C_{m_\psi} - \frac{e_\psi}{e}\,\frac{e}{D}\,C_{Y_\theta}\right)
\end{aligned}
\right\} \qquad (1)
$$

L 1575

It is noted here that the derivation of the foregoing equations may be obtained in the same manner as that given in reference 2 except for the introduction of the ratios I_Y/I_Z' and e_ψ/e because of the existence of separate elastic centers in pitch and yaw. For this system the effective angles of attack given by equation (11) of reference 2 may be rewritten as

$$\bar{\theta} = \theta - \frac{e\dot{\theta}}{V}$$

and

$$\bar{\psi} = \psi - \frac{e_\psi\dot{\psi}}{V}$$

where the barred symbols denote effective angles of pitch and yaw. The corresponding aerodynamic moments in pitch M_Y and yaw M_Z become

$$M_Y = M_{Y,p} - eF_Z$$

$$M_Z' = M_{Z,p} + e_\psi F_Y$$

rather than equations (13) of reference 2, where $M_{Y,p}$ and $M_{Z,p}$ are the aerodynamic moments about pitch and yaw axes in the propeller plane and F_Z and F_Y are vertical and side forces, respectively, acting in the propeller plane. The existence of separate elastic centers also destroys the inertial symmetry that is usually assumed for the case of the common elastic center by introducing the moment of inertia in yaw I_Z' not equal to the moment of inertia in pitch I_Y. The stability of the system is determined from the roots of the following characteristic equation which may be conveniently obtained by applying the Laplace transformation (see ref. 5, for example):

$$F(s) = s^4 + c_3 s^3 + c_2 s^2 + c_1 s + c_0 = 0 \tag{2}$$

where

$$\left.\begin{aligned} c_3 &= a_1 + b_1 \\ c_2 &= a_2 + b_2 + a_1 b_1 + a_3 b_3 \\ c_1 &= a_1 b_2 + a_2 b_1 - a_4 b_3 - a_3 b_4 \\ c_0 &= a_2 b_2 + a_4 b_4 \end{aligned}\right\} \tag{3}$$

Within the range of parameters for the physical system considered in this study, the roots of equation (2) have been found to occur in the complex conjugate pairs

$$s = B_n \pm i\omega_n \qquad (n = 1, 2)$$

where B_n is a total damping coefficient and ω_n the frequency of oscillation. Positive values of B_n indicate an undamped or unstable condition. Two solutions are found for the whirl instability; B_1 and ω_1 are found to correspond to wobbling motions of the propeller shaft around an elliptical path that is traversed in the opposite sense to the

propeller rotation direction whereas B_2 and ω_2 correspond to a wobbling direction that is the same as the propeller rotation.

Exact solutions of equation (2) have been obtained for various combinations of parameters. Values of B_n for the lowest mode have been obtained as a function of ζ_θ and ζ_ψ, and typical plots are shown in figure 2 for the special case of $e_\psi = e$ and $I_Y = I_Z$. The consistently linear trends appearing in the figure suggest the existence of a linear relation between total damping and the damping in the structure. Such a relation may be obtained by the following considerations: Equation (2) is assumed in the factored form

$$\left[(s - B_1)^2 + \omega_1^2\right]\left[(s - B_2)^2 + \omega_2^2\right] = 0$$

corresponding to the complex conjugate roots noted previously. By equating like coefficients in this expression with those in equation (2) and neglecting all terms of B_n of higher order than the first, it is found that

$$B_n = \frac{\omega_n^2}{2}\left(\frac{c_1 - \omega_n^2 c_3}{\omega_n^4 - c_0}\right) \tag{4}$$

where the whirl frequency ω_n is given by

$$\omega_n^2 = \frac{1}{2}\left(c_2 \pm \sqrt{c_2^2 - 4c_0}\right) \tag{5}$$

The negative sign preceding the radical in equation (5) gives ω_1 and the positive sign, ω_2. For all cases studied in this paper and in references 2 and 3, the lower whirl mode (or retrograde mode) corresponding to B_1 and ω_1 has been found to be the critical mode; that is, it occurs at the lowest airplane forward speed.

For the case of neutral stability, defining the borderline condition between damped and undamped motion, $B_1 = 0$, and hence,

$$c_1 - \omega_1^2 c_3 = 0 \tag{6}$$

Substitution in equations (5) and (6) for the c and a values from equations (1) and (3) gives the following linear relations between the damping coefficients in pitch and yaw for neutral stability:

$$2\zeta_\psi = -K_0(2\zeta_\theta) + K_1 \tag{7}$$

where

$$K_0 = \frac{K_2}{\frac{\omega_\psi}{\omega_\theta} K_3} \tag{7a}$$

$$K_1 = \frac{\frac{1}{\mu}\frac{D}{e}\frac{\Omega}{\omega_\theta}\frac{J}{\pi}}{\frac{\omega_\psi}{\omega_\theta} K_3} \left\{ P_1 K_2 + \frac{I_Y}{I_Z'} P_1' K_3 + \frac{I_Y}{I_Z'}\frac{\Omega}{\omega_\theta}\frac{J}{\pi}\left[\frac{I_X \Omega}{I_Y \omega_\theta}\left(P_2 + P_2'\right)\right.\right.$$

$$\left.\left. + \frac{2}{\mu}\frac{\Omega}{\omega_\theta}\frac{J}{\pi}\left(P_2 P_3' + P_2' P_3\right)\right]\right\} \tag{7b}$$

$$K_2 = \left(\frac{\omega_\psi}{\omega_\theta}\right)^2 - \left(\frac{\omega_1}{\omega_\theta}\right)^2 - \frac{1}{\mu}\left(\frac{\Omega}{\omega_\theta}\frac{J}{\pi}\right)^2\left(\frac{e_\psi}{e}\frac{I_Y}{I_Z'}\right) C_{Y_\psi} \tag{7c}$$

$$K_3 = 1 - \left(\frac{\omega_1}{\omega_\theta}\right)^2 - \frac{1}{\mu}\left(\frac{\Omega}{\omega_\theta}\frac{J}{\pi}\right)^2 C_{Y_\psi} \tag{7d}$$

The quantities P_1, P_2, P_3, etc., are propeller aerodynamic terms defined by

$$P_1 = C_{m_q} - 2\left(\frac{e}{D}\right)^2 C_{Y_\psi}$$

$$P_2 = C_{m_\psi} - \frac{e}{D} C_{Y_\theta}$$

$$P_3 = \frac{e_\psi}{e} C_{m_\psi} + \frac{C_{Y_q}}{2} - \frac{e_\psi}{e}\frac{e}{D} C_{Y_\theta}$$

$$P_1' = C_{m_q} - 2\left(\frac{e_\psi}{e}\right)^2\left(\frac{e}{D}\right)^2 C_{Y_\psi}$$

$$P_2' = C_{m_\psi} - \frac{e_\psi}{e}\frac{e}{D} C_{Y_\theta}$$

$$P_3' = C_{m_\psi} + \frac{e_\psi}{e}\frac{C_{Y_q}}{2} - \frac{e_\psi}{e}\frac{e}{D} C_{Y_\theta}$$

The characteristics of these propeller aerodynamic terms will be discussed subsequently. The term $\left(\frac{\omega_1}{\omega_\theta}\right)^2$ is given by

$$\left(\frac{\omega_1}{\omega_\theta}\right)^2 = \frac{1}{2}\left\{1 + \left(\frac{\omega_\psi}{\omega_\theta}\right)^2 + \left(\frac{I_X\Omega}{I_Y\omega_\theta}\right)^2 \frac{I_Y}{I_Z'} + 4\zeta_\theta\zeta_\psi \frac{\omega_\psi}{\omega_\theta} + A_1 - \sqrt{\left[1 + \left(\frac{\omega_\psi}{\omega_\theta}\right)^2 + \left(\frac{I_X\Omega}{I_Y\omega_\theta}\right)^2 \frac{I_Y}{I_Z'} + 4\zeta_\theta\zeta_\psi \frac{\omega_\psi}{\omega_\theta} + A_1\right]^2 - 4\left[\left(\frac{\omega_\psi}{\omega_\theta}\right)^2 + A_0\right]}\right\} \tag{8a}$$

where

$$A_1 = \frac{1}{\mu}\frac{\Omega}{\omega_\theta}\frac{J}{\pi}\left\{-\frac{\Omega}{\omega_\theta}\frac{J}{\pi} C_{Y_\psi}\left(1 + \frac{e_\psi}{e}\frac{I_Y}{I_Z'}\right) - \frac{D}{e}\left(2\zeta_\psi \frac{\omega_\psi}{\omega_\theta} P_1 + 2\zeta_\theta \frac{I_Y}{I_Z'} P_1'\right)\right.$$

$$\left. + \frac{1}{\mu}\frac{\Omega}{\omega_\theta}\frac{J}{\pi}\left(\frac{D}{e}\right)^2 P_1P_1' + 2\frac{I_Y}{I_Z'}\left[\frac{I_X\Omega}{I_Y\omega_\theta}\left(P_3 + P_3'\right) + \frac{2}{\mu}\frac{\Omega}{\omega_\theta}\frac{J}{\pi} P_3P_3'\right]\right\} \tag{8b}$$

$$A_0 = \frac{1}{\mu}\left(\frac{\Omega}{\omega_\theta}\frac{J}{\pi}\right)^2\left[-C_{Y_\psi}\left(\frac{\omega_\psi^2}{\omega_\theta^2} + \frac{e_\psi}{e}\frac{I_Y}{I_Z'}\right) + \frac{1}{\mu}\frac{\Omega}{\omega_\theta}\frac{J}{\pi}\left(C_{Y_\psi}{}^2\frac{e_\psi}{e}\frac{I_Y}{I_Z'} + \frac{D^2}{e^2} P_2P_2'\right)\right] \tag{8c}$$

(In the application of eqs. (7) and (8), it develops that simplified forms can be used, as indicated later in eqs. (13).) If structural damping as considered in reference 2 is assumed in place of viscous damping as assumed herein, the relations $g_\theta = 2\zeta_\theta\left(\frac{\omega_1}{\omega_\theta}\right)$ and $g_\psi = 2\zeta_\psi\left(\frac{\omega_1}{\omega_\psi}\right)$, based on equation (27) of reference 2, are introduced into equations (7).

For the special case of $e_\psi = e$ and $I_Y = I_Z'$, equations (7) are plotted in figure 3 for the three cases considered in figure 2. In calculating ω_1/ω_θ, the terms involving ζ_θ and ζ_ψ in equations (8a) and (8b) were neglected. The circular points represent values of ζ_θ and ζ_ψ crossplotted from figure 2 for $B_1 = 0$ in application of equation (2). These points are included in order to check the adequacy of equations (7) for determining the region of instability, which is the area below the line and bounded by the ordinate and abscissa in a given case. Also compared in figure 3 are the frequency ratios ω_1/ω_θ calculated by equations (2) and (8) for the three values of $\omega_\psi/\omega_\theta$. Equations (7) are seen to predict somewhat steeper slopes and larger values of $2\zeta_\psi$ than does equation (2) and may accordingly be regarded as conservative in the sense that the regions of instability are slightly larger than those of equation (2). Since these differences are small, equations (7) may therefore be considered satisfactory for defining the borderline condition between stability and instability for the range of parameters covered in the present study.

Conditions for Eliminating Regions of Instability

One way for an engine-propeller combination to be free from propeller whirl instability is for the triangular area of instability shown in figure 3 to be eliminated completely. This may be done by simply setting the intercept $K_1 = 0$ in equation (7), so that the linear neutral stability boundary becomes a line through the origin, and the following quadratic equation in $\frac{V}{\frac{D}{2}\omega_\theta}$ is obtained:

$$\left(\frac{V}{\frac{D}{2}\omega_\theta}\right)^2 \frac{1}{\mu}\left(\frac{I_Y}{I_Z'}\right)\left[2\left(P_2P_3' + P_2'P_3\right) - C_{Y_\psi}\left(P_1' + \frac{e_\psi}{e}P_1\right)\right]$$

$$+ \left(\frac{V}{\frac{D}{2}\omega_\theta}\right)\frac{I_Y}{I_Z'}\frac{I_X\Omega}{I_Y\omega_\theta}\left(P_2 + P_2'\right) + P_1\left[\left(\frac{\omega_\psi}{\omega_\theta}\right)^2 - \left(\frac{\omega_1}{\omega_\theta}\right)^2\right] + \frac{I_Y}{I_Z'}P_1'\left[1 - \left(\frac{\omega_1}{\omega_\theta}\right)^2\right] = 0 \tag{9a}$$

The quantity $\left(\frac{\omega_1}{\omega_\theta}\right)^2$ in this equation is obtained from equation (8a) considered without the aerodynamic and damping terms; these additional terms are shown in reference 2 to have a negligible effect on the precessional frequency ω_1 for a system with a common elastic center. Results of sample calculations with equation (9a) are shown in figure 4. As may be seen, satisfactory solutions can be obtained by simply neglecting the quadratic term in V as long as the gyroscopic parameter $\sqrt{\frac{I_Y}{I_Z'}}\left(\frac{I_X\Omega}{I_Y\omega_\alpha}\right)$ is not too small and $\frac{e_\psi}{e}$ is not too large.

For a completely symmetrical system in which $\frac{\omega_\psi}{\omega_\theta} = 1$ and $\frac{e_\psi}{e} = \frac{I_Y}{I_Z'} = 1$, neglect of the quadratic term in equation (9a) and introduction of equations (8) with $A_0 = A_1 = 0$ leads to the following simple stability criterion for a system to be free of propeller whirl instability:

$$-\frac{P_2}{P_1}\frac{V}{\frac{D}{2}\omega_\theta} < \frac{1}{2}\left[\sqrt{4 + \left(\frac{I_X\Omega}{I_Y\omega_\theta}\right)^2} - \frac{I_X\Omega}{I_Y\omega_\theta}\right] \tag{9b}$$

where it may be noted that the aerodynamic terms are on the left-hand side of the equation, and the right-hand side contains only mechanical terms. For small values of $\frac{I_X\Omega}{I_Y\omega_\theta}$ equation (9b) reduces to equation (26) of reference 2 when the damping coefficient $\tilde{g}_{\theta_2}$ equals zero.

Divergence Equation

The conditions for neutral stability with respect to static divergence is obtained from equation (2) by letting $s = 0$ so that

$$c_0 = a_2b_2 + a_4b_4 = 0 \tag{10}$$

From the definitions of a_2, b_2, a_4, and b_4 given in equation (1) the following quadratic equation may be obtained:

$$P_D^4 - P_D^2E + G = 0 \tag{11}$$

where the divergence parameter $P_D^2 = \kappa\left(\frac{\Omega}{\omega_\theta}\frac{J_D}{\pi}\right)^2 = \kappa\left(\frac{J_D}{\frac{D}{2}\omega_\theta}\right)^2$ with

$$\kappa = \frac{1}{\mu}\frac{D}{e} = \frac{\pi\rho D^5}{32 I_Y}$$

and

$$E = \frac{\frac{e}{D} C_{Y_\psi}\left[\left(\frac{\omega_\psi}{\omega_\theta}\right)^2 + \frac{e_\psi}{e}\frac{I_Y}{I_Z'}\right]}{\frac{I_Y}{I_Z'}\left[\left(\frac{e}{D} C_{Y_\psi}\right)^2 \frac{e_\psi}{e} + P_2 P_2'\right]}$$

$$G = \frac{\left(\frac{\omega_\psi}{\omega_\theta}\right)^2}{\frac{I_Y}{I_Z'}\left[\left(\frac{e}{D} C_{Y_\psi}\right)^2 \frac{e_\psi}{e} + P_2 P_2'\right]}$$

The application of equation (11) is discussed in the following section along with the dynamic whirl equations. However, at this point, it may be worth noting that, when $\frac{\omega_\psi}{\omega_\theta} = 1$ and $\frac{e_\psi}{e} = \frac{I_Y}{I_Z'} = 1$, equation (10) becomes

$$a_2^2 + a_4^2 = 0$$

which obviously has no real roots unless a_2 and a_4 are both zero. However, the condition that a_4 be zero (except for the trivial case of $P_D = 0$) when combined with $a_2 = 0$ yields

$$P_D^2 = \frac{C_{Y_\theta}}{C_{m_\psi} C_{Y_\psi}} \tag{12}$$

It should be noted in this equation that for each value of J, there is just one value of $\frac{e}{D}$, given by $\frac{e}{D} = \frac{C_{m_\psi}}{C_{Y_\theta}}$, for which divergence can occur.

Note also that if C_{Y_θ} is assumed to be zero, a_4 cannot be zero unless C_{m_ψ} is zero, which in turn requires J to be zero. Thus, for a completely symmetrical engine-propeller combination, divergence based solely on Ribner coefficients (ref. 4) cannot occur.

APPLICATION OF WHIRL STABILITY AND DIVERGENCE EQUATIONS

With the exception of the results given in figure 2, most of the propeller-whirl trends presented in this paper were obtained by use of equations (7) for the ranges of dimensionless parameters listed in table I for the case of the common elastic center $\left(\frac{e_\psi}{e} = \frac{I_Y}{I_{Z'}} = 1\right)$. A few calculations were performed for the case of separate elastic centers using the tabulated values of $\frac{e_\psi}{e}$ and $\frac{I_Y}{I_{Z'}}$ which were selected arbitrarily. The choice of the remaining parameters in table I was largely influenced by a compilation of available (though, unfortunately, incomplete) information on pertinent engine-propeller characteristics on a number of piston-engine and turbopropeller power plants in service over a number of years. Most of the propeller aerodynamic coefficients used in these calculations are based on the blade characteristics of the same propeller used in references 2 and 3 and currently in service on commercial air transports. These blade characteristics are reproduced from reference 2 in figure 5(a), and the propeller is designated as propeller A. Some calculations based on the blade characteristics of propeller B, also shown in figure 5, were performed. These characteristics apply to a propeller that was widely used from 1945 to 1950. The ranges of propeller advance ratio J and blade angle at the 3/4 radius $(\beta_{0.75R})$ are shown in figure 5(b) for both propellers for the windmilling (or nonthrusting) condition.

The propeller aerodynamic coefficients based on the propeller characteristics shown in figures 5(a) and 5(b) are listed in table II. The side-force coefficient with respect to pitch C_{Y_θ}, which is not given by Ribner in reference 4 but is approximated in references 2 and 3, was omitted in all but a few calculations concerned with the case of the separate elastic centers, with divergence, and for the parametric relation for systems free of propeller whirl, given by equation (9a). Values of C_{Y_θ} given in table II were obtained from reference 2 by following the approximate scheme given therein.

L-1575

Before presenting analytical trends in propeller whirl boundaries, it is worth noting the following acceptable approximations to the slope K_0 and intercept K_1 in equations (7) which arise from the negligible effect of propeller aerodynamic coefficients on the whirl frequency:

$$K_0 \approx \frac{\left(\frac{\omega_\psi}{\omega_\theta}\right)^2 - \left(\frac{\omega_1}{\omega_\theta}\right)^2}{\frac{\omega_\psi}{\omega_\theta}\left[1 - \left(\frac{\omega_1}{\omega_\theta}\right)^2\right]} \tag{13a}$$

$$K_1 \approx \frac{\frac{1}{\mu}\frac{D}{e}\frac{\Omega}{\omega_\theta}\frac{J}{\pi}}{\frac{\omega_\psi}{\omega_\theta}\left[1 - \left(\frac{\omega_1}{\omega_\theta}\right)^2\right]} \left\{ P_1 \left[\left(\frac{\omega_\psi}{\omega_\theta}\right)^2 - \left(\frac{\omega_1}{\omega_\theta}\right)^2\right] + \frac{I_Y}{I_Z'} P_1' \left[1 - \left(\frac{\omega_1}{\omega_\theta}\right)^2\right] \right.$$

$$\left. + \frac{I_Y}{I_Z'} \frac{I_X \Omega}{I_Y \omega_\theta} \frac{\Omega}{\omega_\theta} \frac{J}{\pi}(P_2 + P_2') \right\} \tag{13b}$$

where

$$\left(\frac{\omega_1}{\omega_\theta}\right)^2 \approx \frac{1}{2}\left\{1 + \left(\frac{\omega_\psi}{\omega_\theta}\right)^2 + \frac{I_Y}{I_Z'}\left(\frac{I_X \Omega}{I_Y \omega_\theta}\right)^2 - \sqrt{\left[1 + \left(\frac{\omega_\psi}{\omega_\theta}\right)^2 + \frac{I_Y}{I_Z'}\left(\frac{I_X \Omega}{I_Y \omega_\theta}\right)^2\right]^2 - 4\left(\frac{\omega_\psi}{\omega_\theta}\right)^2}\right\} \tag{13c}$$

Cases in which the effect of propeller aerodynamics on whirl frequency is not negligible are illustrated in figure 6 for extreme values of $\frac{\omega_\psi}{\omega_\theta}$ and $\frac{e}{D}$. However, even for these cases the corresponding effects on the neutral stability boundaries are still small.

Parametric Whirl Instability Trends

In determining the effects of the various dimensionless parameters on propeller whirl, the condition of symmetry in damping has been chosen

in most cases. A few cases have been examined for extreme unsymmetrical conditions. The trends for the system with a common elastic center are presented first, except as noted below for the effect of $\frac{\Omega}{\omega_\theta}$ on whirl frequency.

Effect of rotational-to-pitch frequency ratio $\frac{\Omega}{\omega_\theta}$.- Initial consideration is given to $\frac{\Omega}{\omega_\theta}$ because it relates the propeller rotational speed to engine-nacelle stiffness and is used as a basis for evaluating other parameters. The effect of this parameter on whirl frequency is shown in different forms in references 2 and 3. In the present paper $\frac{\Omega}{\omega_\theta}$ is combined with the inertia ratios $\frac{I_X}{I_Y}$ and $\sqrt{\frac{I_Y}{I_Z'}}$ into an angular momentum ratio $\sqrt{\frac{I_Y}{I_Z'}}\left(\frac{I_X\Omega}{I_Y\omega_\theta}\right)$, and the effect of this gyroscopic parameter on the natural whirl frequency is shown in figure 7 for both forward and retrograde whirl modes of the system for the general case of separate elastic centers in pitch and yaw.

Figure 8 is a stability chart in which the damping coefficient 2ζ is shown as a function of J for various values of $\frac{\omega_\psi}{\omega_\theta}$. Four values of $\frac{\Omega}{\omega_\theta}$ are shown. The parameters held constant are $\frac{1}{\mu} = 0.00978$, $\frac{I_X}{I_Y} = 0.1184$, $\frac{e}{D} = 0.235$. The values selected for these parameters are considered to be in the center of the range of values of current interest. Variations in each of these values in turn are studied for fixed values of the remaining parameters, and these variations are made with $\frac{\omega_\psi}{\omega_\theta} = 1$ (the solid curves labeled a, b, c, and d).

Figure 8 shows that the regions of instability increase with increasing $\frac{\Omega}{\omega_\theta}$ and with increasing J. Negative values of 2ζ in figure 8 indicate conditions completely free of propeller whirl instability. It is evident that $\frac{\Omega}{\omega_\theta}$ can be low enough for the system to be stable throughout the range of values of J.

Effect of yaw-to-pitch frequency ratio $\frac{\omega_\psi}{\omega_\theta}$.- This is one of the fixed parameters in figures 9 to 11. An indication of the effect of

frequency ratio itself with other parameters held fixed can be obtained by examination of figure 8. As $\frac{\Omega}{\omega_\theta}$ is increased, the regions of instability defined by frequency ratios less than 1 tend to become somewhat larger than the regions at frequency ratio 1. For $\frac{\Omega}{\omega_\theta} < 2.5$ the instability region at $\frac{\omega_\psi}{\omega_\theta} = 1.0$ is greater than the regions for the other frequency ratios, but for $\frac{\Omega}{\omega_\theta} \geqq 2.5$ a reversal of this trend is indicated for $\frac{\omega_\psi}{\omega_\theta} < 1$. Further consideration of frequency-ratio effect is discussed later in connection with divergence.

Effect of inertia-density ratio $\frac{1}{\mu}$.- The effect of inertia-density ratio is shown in figure 9. The curves labeled a, b, c, and d are the same as curves a, b, c, and d of figure 8. The increasing region of instability with larger values of $\frac{1}{\mu}$ indicates that for a given engine-propeller combination more structural damping is required to stabilize the system at lower altitudes than at higher altitudes. It is also evident that an undamped system is essentially insensitive to inertia-density ratio, and a small amount of structural damping has a strong stabilizing effect at low values of inertia-density ratio. These effects are similar to those found in reference 3 in which density was part of a mass-density ratio based on the mass of the propeller.

Effect of polar-to-pitch moment-of-inertia ratio $\frac{I_X}{I_Y}$.- Figure 10 shows effects of $\frac{I_X}{I_Y}$, about the same curves a, b, c, and d, on the region of instability, and it is evident that more damping is required for stability as the magnitude of $\frac{I_X}{I_Y}$ increases. An increase in inertia ratio may be visualized as being caused by shortening the engine for a given propeller, or using a heavier propeller on a given engine.

Effect of $\frac{e}{D}$.- This parameter relates the propeller diameter and the moment arm between the plane of the propeller and the effective elastic center of the system. Figure 11 shows that the smaller the value of $\frac{e}{D}$, the greater the amount of structural damping required for stability. This result is essentially the same as that found in references 2 and 3. Decreasing $\frac{e}{D}$ for a given propeller is equivalent to

moving the elastic center closer to the propeller plane or to increasing the propeller diameter for a fixed elastic center location. With less damping required as $\frac{e}{D}$ is raised, it is evident that $\frac{e}{D}$ can be high enough for the system to be free from propeller whirl throughout the J-range. It is shown later, however, that the extent to which $\frac{e}{D}$ can be raised actually is limited by the divergence boundary.

It should be noted that the effects shown in figure 11 are aerodynamic effects, since it has been assumed that $\frac{e}{D}$ can be changed without affecting either the polar or pitching moments of inertia of the system. However, when the inertial change was accounted for (due to changing the moment arm e), the regions of instability were only slightly enlarged from those shown in figure 11; thus the dominance of the aerodynamic effect of varying $\frac{e}{D}$ is indicated.

L 1 5 7 5

Effect of thrust coefficient.- Most of the trends presented in this paper apply to the windmilling case, that is, the case of zero thrust ($T_c = 0$), and the work of reference 2 has shown thrust to have a minor effect on the propeller-whirl neutral stability boundaries. Brief attention was also given to this matter in the present study, and some results of varying T_c from -0.01 to 0.036 are shown as a function of $\frac{\Omega}{\omega_\theta}$ in figure 12. Variation of thrust coefficient over this range either positive or negative is seen to have a small effect on the region of instability.

Analytical trends for a different propeller.- As previously noted, most of the work reported in this paper is based on the blade characteristics and advance ratios for propeller A as given in figures 5(a) and 5(b). Neutral stability boundaries and whirl frequencies based on the blade characteristics and advance ratios for propeller B are compared in figure 13 with stability boundaries and whirl frequencies for propeller A. The results of the calculations show a somewhat smaller region of instability for propeller B than for propeller A at a low value of $\frac{\Omega}{\omega_\theta}$ and as $\frac{\Omega}{\omega_\theta}$ increases, the sizes of the instability regions for the two propellers become indistinguishable. The distinction between the two propellers appears to be even less significant insofar as whirl frequency (shown in ratio form in the lower part of the figure) is concerned.

Effects of unsymmetrical damping.- Up to this point only the case of symmetrical damping has been considered (that is, $\zeta_\psi = \zeta_\theta$ as previously noted). When the damping coefficients in pitch and yaw are unequal, more damping in the mode having the lower stiffness is required for neutral stability (that is, more damping in pitch is required for

$\frac{\omega_\psi}{\omega_\theta} < 1$, and conversely, more damping in yaw than in pitch is required for $\frac{\omega_\psi}{\omega_\theta} > 1.0$). This situation is evident in figure 3 and is also shown in figure 14 for the full J-range of propeller A for the extreme cases in which the damping in first one degree of freedom and then the other is assumed to be zero. The fixed parameters for these curves are the same as those in figure 8, and the reference curves b, c, and d for figure 8 are reproduced in figure 14. As may be seen, the frequency ratio does not have to be very far from unity for the damping required for neutral stability to be quite large when the damping in one of the modes is completely eliminated. This result is somewhat similar to that found in reference 2 for less extreme damping ratios.

L
1
5
7
5

Effect of separate elastic centers in pitch and yaw.- The parametric whirl trends presented up to this point have been based on a common elastic center. The results of some calculations for the case of separate elastic centers in pitch and yaw are shown in figure 15. The moment arm ratio $\frac{e_\psi}{e}$ was arbitrarily varied from 0.2 to 2.0, and for each value of this ratio chosen, a corresponding value of the inertia ratio $\frac{I_Z'}{I_Y}$ was determined by using inertial characteristics representative of an engine-propeller system currently operational. The solid curves, which were determined by use of the approximate relations given by equations (13) for $\frac{e_\psi}{e} = \frac{I_Z'}{I_Y} = 1$ are designated by a', b', and so forth, to denote the fact that they are essentially the reference curves a, b, c, and d but are based on the nonzero values of C_{Y_θ} given in table II. A comparison of the solid with the dashed curves shows an increase in the region of instability for $\frac{e_\psi}{e} < 1$ and a decrease in the region of instability for $\frac{e_\psi}{e} > 1$ as $\frac{\Omega}{\omega_\theta}$ increases.

Analytical Divergence Trends and Comparison With Whirl Trends

Divergence boundaries calculated by use of equations (11) and (12) are presented in figures 16 to 18 and are compared with whirl trends in figure 19.

Divergence.- In figure 16 the divergence parameter $P_D = \frac{V_D}{\frac{D}{2}\omega_\theta}\sqrt{\kappa}$ is shown as a function of $\frac{e}{D}$ for three advance ratios and a wide range

of stiffness ratios $\left(\frac{\omega_\psi}{\omega_\theta}\right)^2$. The region of instability lies within the semiclosed curves for all stiffness ratios, the region being largest for extreme stiffness ratios and decreasing as the stiffness ratio approaches one. At stiffness ratios not far from 1 the curves close, and the divergence region becomes a narrow elongated band bounded by an upper as well as a lower positive value of $\frac{e}{D}$ (as, for example, in the case of $\left(\frac{\omega_\psi}{\omega_\theta}\right)^2 = 0.9$ in the lower right plot). At a stiffness ratio of 1 for the case of the common elastic center, this region shrinks to a point which, as previously noted, is determined by equation (12) for each value of J and corresponding nonzero value of the lift-lag coefficient C_{Y_θ}. Increasing J results in an increase in the region of instability and extends it to lower values of $\frac{e}{D}$; this change is equivalent to shortening the distance between the propeller plane and the elastic center. It may also be noted in figure 16 that the effect of a nonzero value of C_{Y_θ}, compared with that for $C_{Y_\theta} = 0$, is to increase the size of the divergence region by an amount that increases as the stiffness ratio gets closer to 1. This effect is opposite to that found for propeller whirl in reference 3. In other words, the inclusion of the lift-lag term in the divergence and whirl equations has the effect of destabilizing an engine-propeller combination in divergence and stabilizing it in whirl.

The divergence behavior at a stiffness ratio of 1 of both propellers considered in this study is shown for the case of the common elastic center in figure 17, which is a plot of equation (12). As may be seen, the divergence speed parameter for propeller B is somewhat higher than that for propeller A.

For the case of separate elastic centers the regions of divergence instability have the same general shapes as those shown in figure 16. For zero stiffness ratio, the values of $\frac{e}{D}$ where P_D is a maximum shift to the right for $\frac{e_\psi}{e} < 1$ and to the left for $\frac{e_\psi}{e} > 1$, and the maximum value of P_D decreases for $\frac{e_\psi}{e} < 1$ and increases for $\frac{e_\psi}{e} > 1$. At a stiffness ratio of 1, divergence occurs at more than one value of $\frac{e}{D}$ as is shown in figure 18, which also shows the region of divergence instability to lie within semiclosed regions for $\frac{e_\psi}{e} < 1$ and within completely closed regions for $\frac{e_\psi}{e} > 1$. Moreover, for $\frac{e_\psi}{e} > 1$ divergence

occurs at values of P_D that are somewhat lower than the single value of P_D at $\frac{e_\psi}{e} = 1$. At other stiffness ratios, divergence regions are completely closed between a range of stiffness ratios that is small for low values of $\frac{e_\psi}{e}$ and increases rapidly as $\frac{e_\psi}{e}$ increases. (See, for example, table III for $J = 2.65$.) Outside of this range of stiffness ratios the divergence regions are semiclosed as in figures 16 and 18.

Comparison between divergence and whirl boundaries.- Whirl boundaries are compared with divergence boundaries for the case of the common elastic center in figure 19 for a wide range of frequency ratios and two widely separated values of $\frac{e}{D}$. The divergence boundaries are seen to be well above the whirl boundaries except at low frequency ratios where both boundaries intersect. The whirl boundaries apply to both damped and undamped systems and the lift-lag term Cy_θ has been omitted from the divergence as well as the whirl calculations. The figure shows divergence rather than whirl to be critical for a system considerably weak in yaw relative to pitch $\left(\text{corresponding to low } \frac{\omega_\psi}{\omega_\theta}\right)$, the divergence region extending further into the whirl region as $\frac{e}{D}$ increases.

Remarks on Effect of Viscous Damping

The stabilizing effect of viscous damping on propeller whirl has been considered both in this paper and in references 2 and 3 along with the effects of other significant parameters. The whirl trends shown in figure 19 for various nonzero damping coefficients are considered worthy of added observations with respect to frequency ratio and $\frac{e}{D}$. The trends indicate that for a given $\frac{e}{D}$ the effect of damping is about the same at all frequency ratios and becomes greater for $\frac{\omega_\psi}{\omega_\theta} \geqq 1.0$ as the distance between the propeller plane and effective elastic center decreases (that is, as $\frac{e}{D}$ decreases). Only at the low frequency ratios near the divergence boundaries does the damping effect tend to diminish, as indicated by the convergent tendencies both of the neutral stability boundaries in the upper part of the figure, and particularly, of the frequency trends in the lower part of the figure. Note also that the damping required to stabilize the system with lower $\frac{e}{D}$ is roughly more than twice as much

as that required to the system with higher $\frac{e}{D}$ at nearly all frequency ratios $\frac{\omega_\psi}{\omega_\theta}$. This behavior is consistent with the effect of $\frac{e}{D}$ and damping noted earlier for a frequency ratio of 1.

CONCLUDING REMARKS

An analytical trend study that extends previous works by Reed, Bland, and Houbolt (NASA TN D-659 and IAS Paper No. 61-34) on propeller whirl instability is reported herein. Most of the present effort is concerned with applications of simple linear equations defining the borderline conditions between stable and unstable motion in terms of viscous damping coefficients in pitch and yaw. Results of these applications are shown for wide ranges of the significant whirl parameters in a number of figures summarizing the analytical trends. These results confirm the results of previous studies in indicating the strong dependence of propeller whirl instability on stiffness, damping, and elastic center (or pivot location) of simplified engine-propeller combinations cantilevered at their elastic centers. In addition, the following conclusions appear to be justified:

L 1 5 7 5

1. Increasing the polar-to-pitch (or yaw) moment-of-inertia ratio increases the region of propeller whirl instability.

2. Aerodynamic effects on the frequency of propeller whirl instability are found to have a small effect on the neutral stability boundaries even at extreme values of yaw-to-pitch frequency ratio. The aerodynamic effects are also small when the distance between the propeller plane and the effective elastic center is large relative to the propeller diameter.

3. For an engine-propeller system with different elastic centers in pitch and yaw, the region of whirl instability tends to decrease when the distance from the propeller plane to the most rearward elastic center is increased. Conversely, the instability region tends to increase as the distance from the propeller plane to the most forward elastic center decreases.

4. The occurrence of engine-propeller divergence at speeds less than the critical whirl speed is unlikely unless the system becomes very weak in one direction (that is, pitch or yaw) relative to another. If the side-force coefficient with respect to pitch angle is omitted in the calculations, divergence cannot occur for a completely symmetrical system (that is, one for which stiffnesses as well as moments of inertia

are respectively equal in the pitch and yaw directions, and the system has a common elastic center).

5. Whereas an engine-propeller system with a common elastic center and equal stiffnesses in pitch and yaw diverges for each advance ratio at just one value of the ratio of the distance between the propeller plane and the elastic center to the propeller diameter, the system with separate elastic centers diverges over a wide range of this ratio for each advance ratio.

Langley Research Center,
National Aeronautics and Space Administration,
Langley Air Force Base, Va., December 15, 1961.

REFERENCES

1. Taylor, E. S., and Browne, K. A.: Vibration Isolation of Aircraft Power Plants. Jour. Aero. Sci., vol. 6, no. 2, Dec. 1938, pp. 43-49.

2. Reed, Wilmer H., III, and Bland, Samuel R.: An Analytical Treatment of Aircraft Propeller Precession Instability. NASA TN D-659, 1961.

3. Houbolt, John C., and Reed, Wilmer H., III: Propeller-Nacelle Whirl Flutter. Paper No. 61-34, Inst. Aerospace Sci., Jan. 1961.

4. Ribner, Herbert S.: Propellers in Yaw. NACA Rep. 820, 1945. (Supersedes NACA ARR 3L09.)

5. Churchill, Ruel V.: Modern Operational Mathematics in Engineering. McGraw-Hill Book Co., Inc., 1944.

TABLE I.- RANGES OF DIMENSIONLESS PROPELLER WHIRL PARAMETERS COVERED IN INVESTIGATION

$\frac{1}{\mu}$	0.0036 to 0.04
$\frac{I_X}{I_Y}$	0 to 0.33
$\frac{e}{D}$ for whirl	0.125 to 0.8545
$\frac{e}{D}$ for divergence	0 to 3.52
$\frac{\omega_\psi}{\omega_\theta}$ for whirl	0.1 to 2.0
$\frac{\Omega}{\omega_\theta}$ (each value fixed for range of J; for example, see fig. 8)	1.26 to 3.15
$\frac{\Omega}{\omega_\theta}$ (for fixed J; for whirl solutions shown in fig. 19)	Variable to 10
$\frac{e_\psi}{e}$ (see fig. 15)	0.2 to 2.0
$\frac{I_{Z'}}{I_Y}$ (see fig. 15)	1.0 to 1.605
T_c	-0.01 to 0.036

TABLE II.- ADVANCE RATIOS AND PROPELLER AERODYNAMIC COEFFICIENTS

FOR WINDMILLING PROPELLERS (T_c = 0)

J	Propeller A					Propeller B				
	C_{Y_ψ}	C_{m_ψ}	C_{m_q}	C_{Y_q}	C_{Y_θ} (a)	C_{Y_ψ}	C_{m_ψ}	C_{m_q}	C_{Y_q}	C_{Y_θ} (a)
1.1						0.2475	0.09643	-0.13665	-0.1799	0.0522
1.48	0.3220	0.1227	-0.1230	-0.2315	0.0706					
1.65						.3144	.09191	-.0948	-.1745	.0617
1.8	.3756	.1184	-.09571	-.2256	.081					
2.15	.41515	.11245	-.07676	-.2161	.084					
2.35						.3719	.08068	-.06136	-.1555	.06995
2.65	.4555	.1033	-.0577	-.2010	.085					
2.8						.3964	.07271	-.04905	-.14105	.0714
3.33						.4177	.06399	-.03601	-.1248	.0711
3.45	.5000	.0888	-.0397	-.1737	.088					
4.08						.4356	.05367	-.02934	-.1052	.0701
4.2	.5285	.0747	-.0292	-.1479	.092					

[a]Calculated by approximation given in reference 2; all other coefficients calculated by reference 4.

Blade Angle for Thrusting Propellers
(Propeller A; J = 2.65)

T_c	$\beta_{0.75R}$
-0.01	43.5°
0	46
.036	58

TABLE III.- RANGES OF STIFFNESS RATIO $\left(\frac{\omega_\psi}{\omega_\theta}\right)^2$ WHICH INCLUDE CLOSED REGIONS OF DIVERGENCE INSTABILITY FOR A SYSTEM WITH SEPARATE ELASTIC CENTERS IN PITCH AND YAW

[J = 2.65; propeller A]

$\frac{e_\psi}{e}$	$\frac{I_Z'}{I_Y}$	$\left(\frac{\omega_\psi}{\omega_\theta}\right)^2$	
		Lower limit	Upper limit
0.2	1.385	0.100	0.209
.5	1.15	.301	.628
1.0	[a]1.0	.692	1.445
1.5	1.151	.902	1.88
2.0	1.605	.863	1.80

[a] $\frac{I_Z'}{I_Y} = \frac{I_Z}{I_Y}$ for common elastic center.

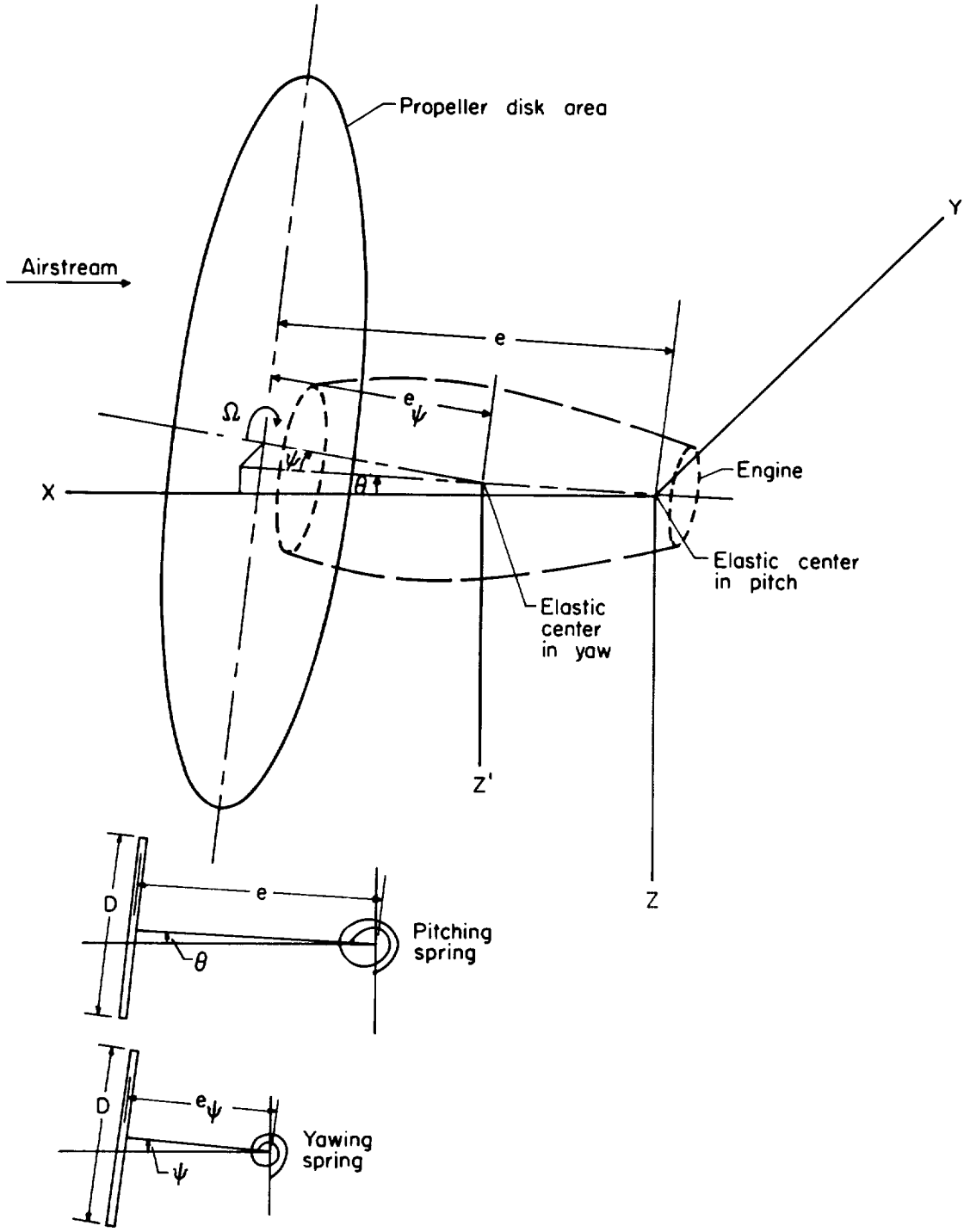

Figure 1.- Idealized engine-propeller system. Directions indicated are considered positive.

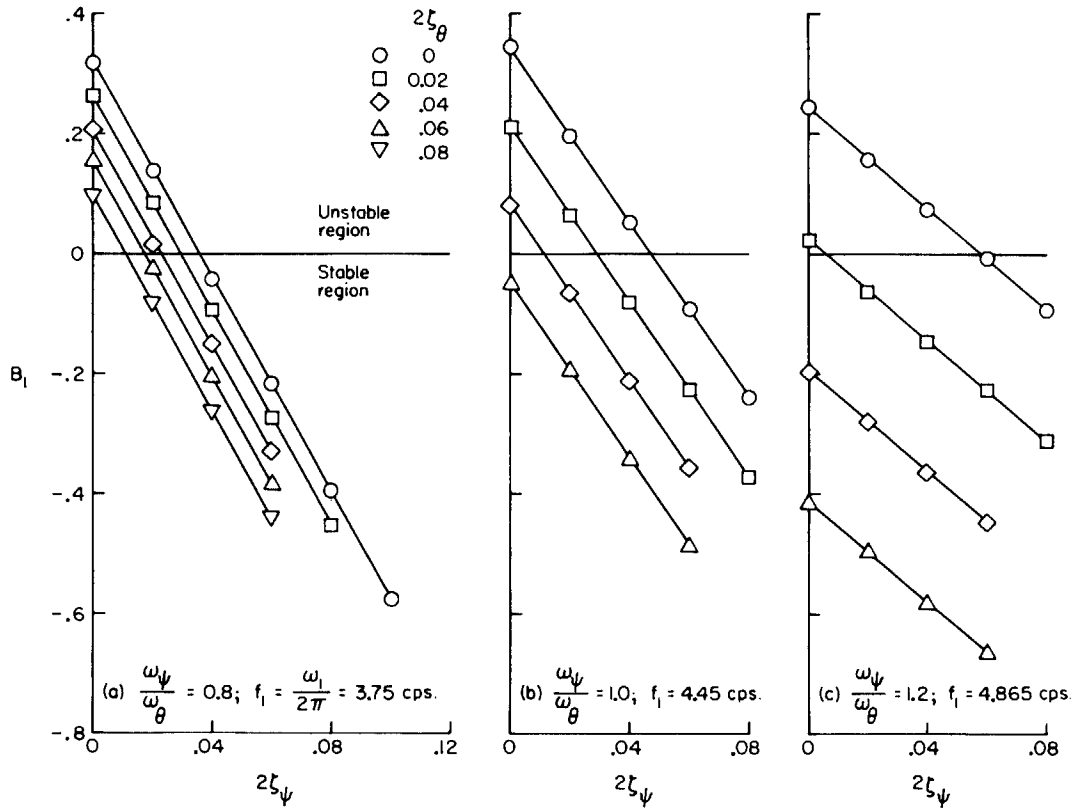

Figure 2.- Typical solutions of quartic stability equation (eq. (2)) for propeller A. $T_c = 0$; $J = 2.65$; $C_{Y_\theta} = 0$; $\frac{e_\psi}{e} = \frac{I_Z}{I_Y} = 1$; $\frac{1}{\mu} = 0.00978$; $\frac{e}{D} = 0.235$; $\frac{I_X}{I_Y} = 0.1184$; $\frac{\Omega}{\omega_\theta} = 3.15$; $\rho = 0.001401$ lb-sec^2/ft^4; $I_Y = 1{,}475$ ft-lb sec^2; D = 13.5 ft; e = 3.17 ft; $\eta = \frac{\Omega}{2\pi} = 17$ rps; $f_\theta = \frac{\omega_\theta}{2\pi} = 5.4$ cps; V = 605 ft/sec.

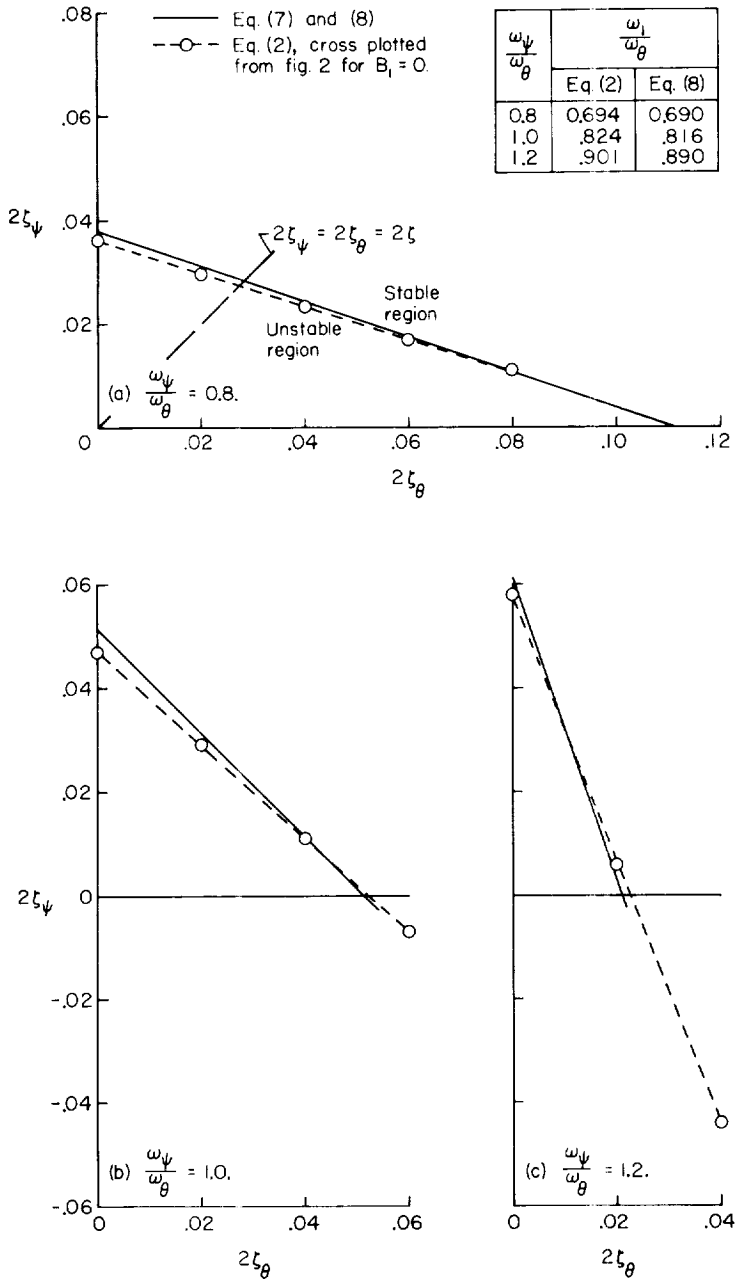

$\frac{\omega_\psi}{\omega_\theta}$	$\frac{\omega_1}{\omega_\theta}$	
	Eq. (2)	Eq. (8)
0.8	0.694	0.690
1.0	.824	.816
1.2	.901	.890

Figure 3.- Typical solutions of linear equation for neutral stability (eqs. (7)) of propeller A. $T_c = 0$; $J = 2.65$; $C_{Y_\theta} = 0$; $\frac{e_\psi}{e} = \frac{I_Z}{I_Y} = 1$; $\frac{1}{\mu} = 0.00978$; $\frac{e}{D} = 0.235$; $\frac{I_X}{I_Y} = 0.1184$; $\frac{\Omega}{\omega_\theta} = 3.15$.

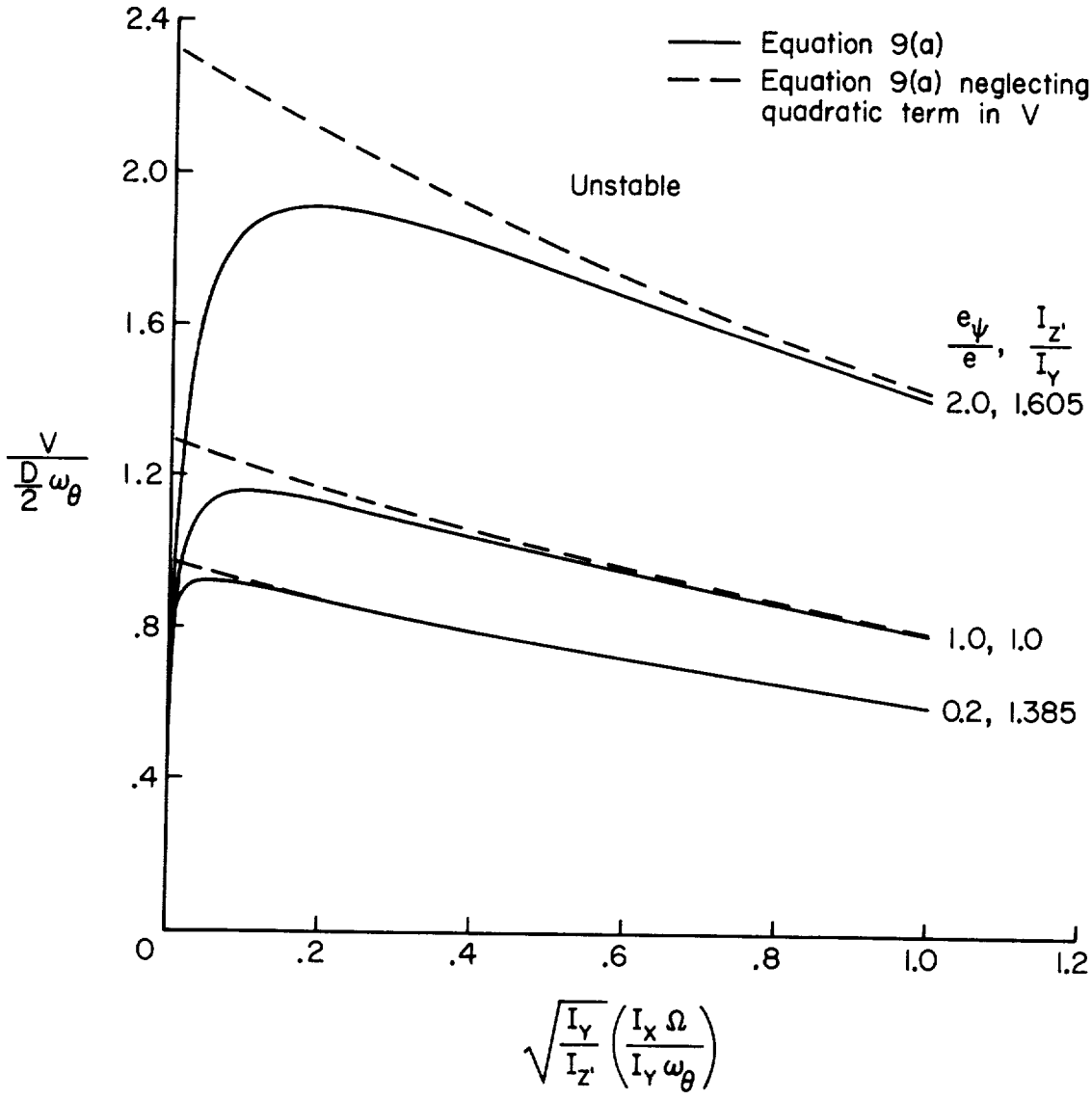

Figure 4.- Propeller whirl boundaries for an undamped system (plot of eq. (9a)) for propeller A with $T_c = 0$; $J = 2.65$; $\left(\frac{\omega_\psi}{\omega_\theta}\right)^2 = 1$; $\frac{l}{\mu} = 0.00978$; $\frac{e}{D} = 0.235$.

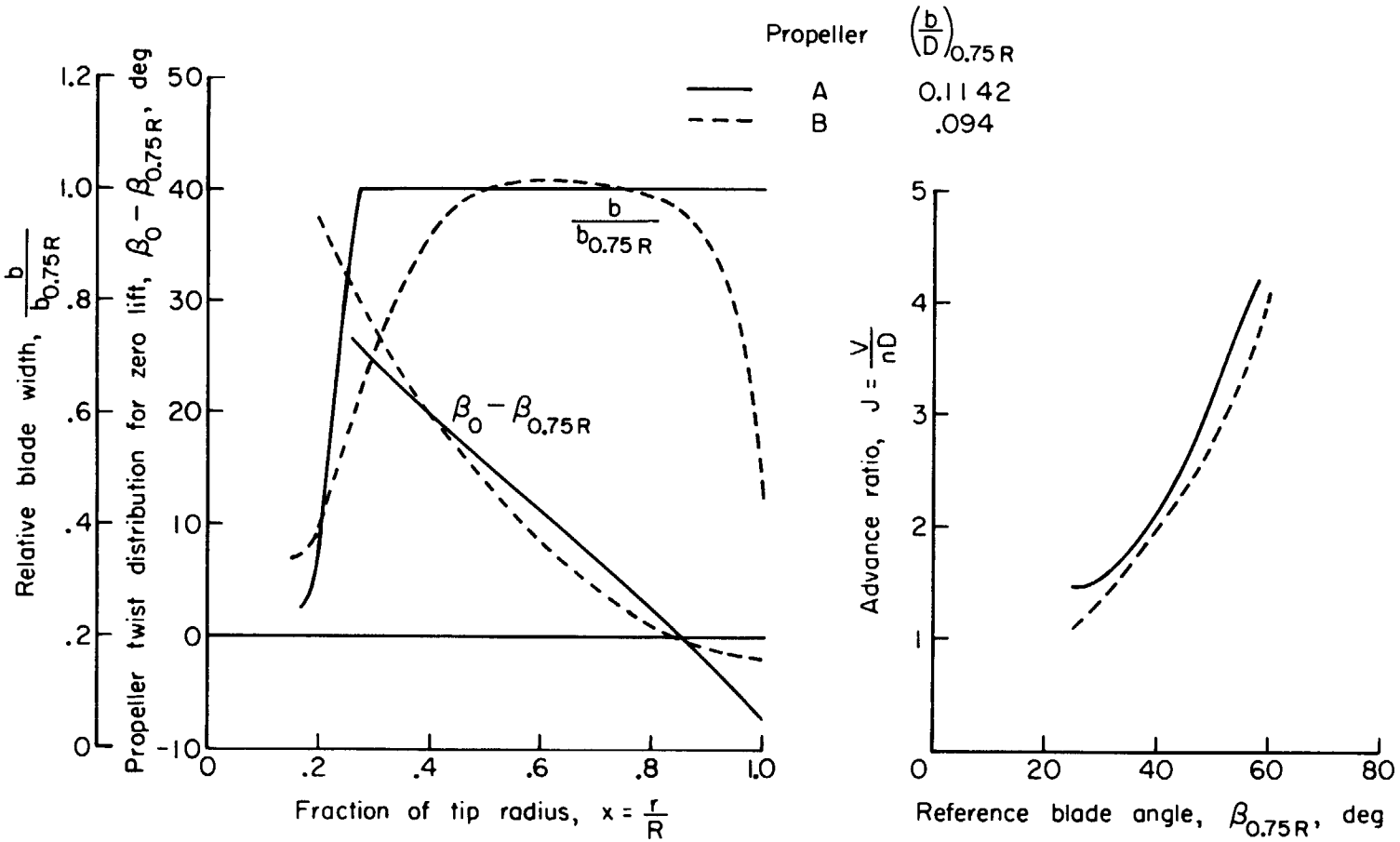

(a) Propeller blade geometrical characteristics.

(b) Variation of advance ratio with reference blade angle for windmilling propellers ($T_c = 0$).

Figure 5.- Propeller blade characteristics used in propeller whirl analytical trend studies (both propellers have 4 blades).

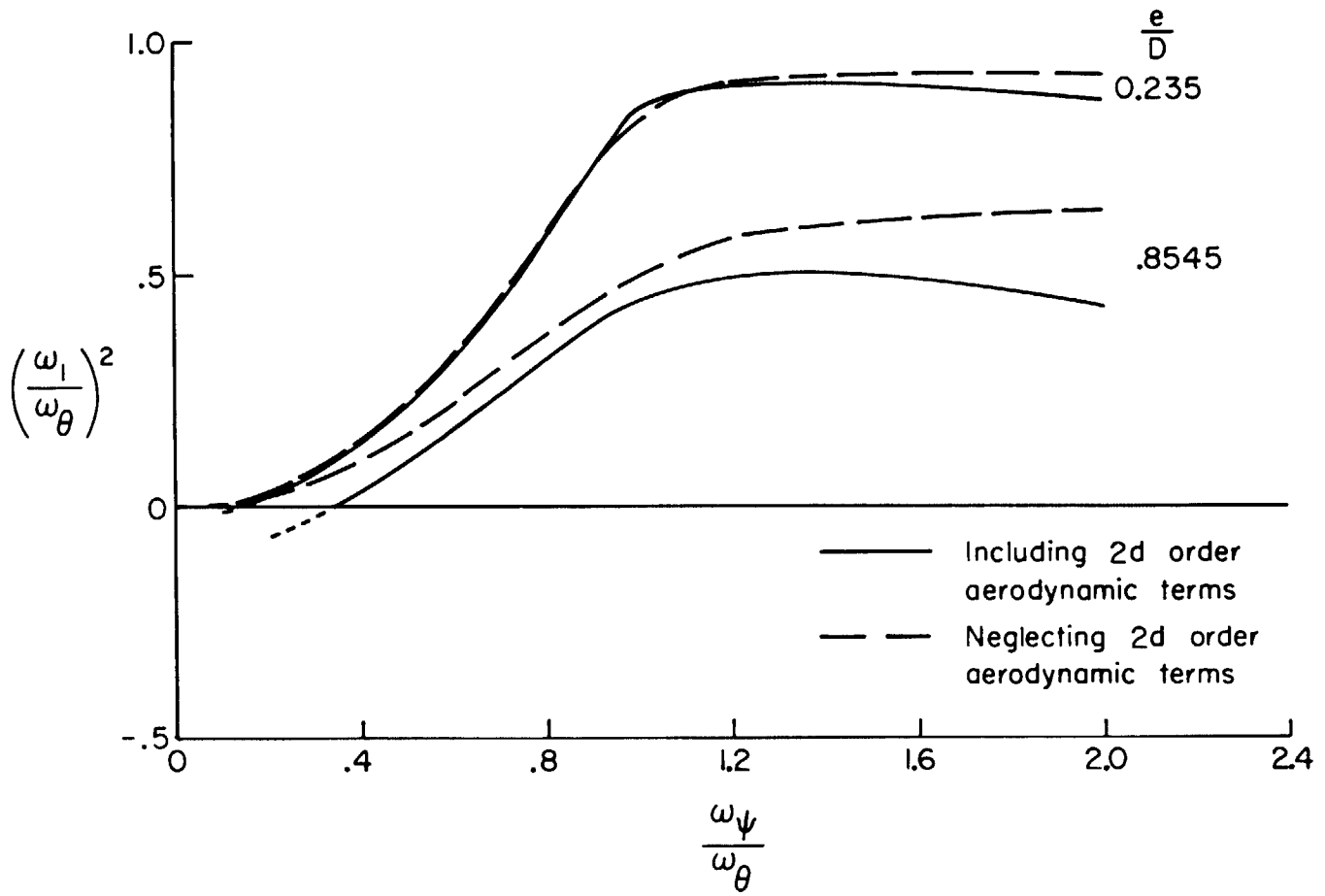

Figure 6.- Whirl frequency trends for propeller A over a wide range of frequency ratios. $T_c = 0$; $J = 2.65$; $C_{Y_\theta} = 0$; $\frac{e_\psi}{e} = \frac{I_Z}{I_Y} = 1$; $\frac{1}{\mu} = 0.00978$; $\frac{I_X}{I_Y} = 0.1184$.

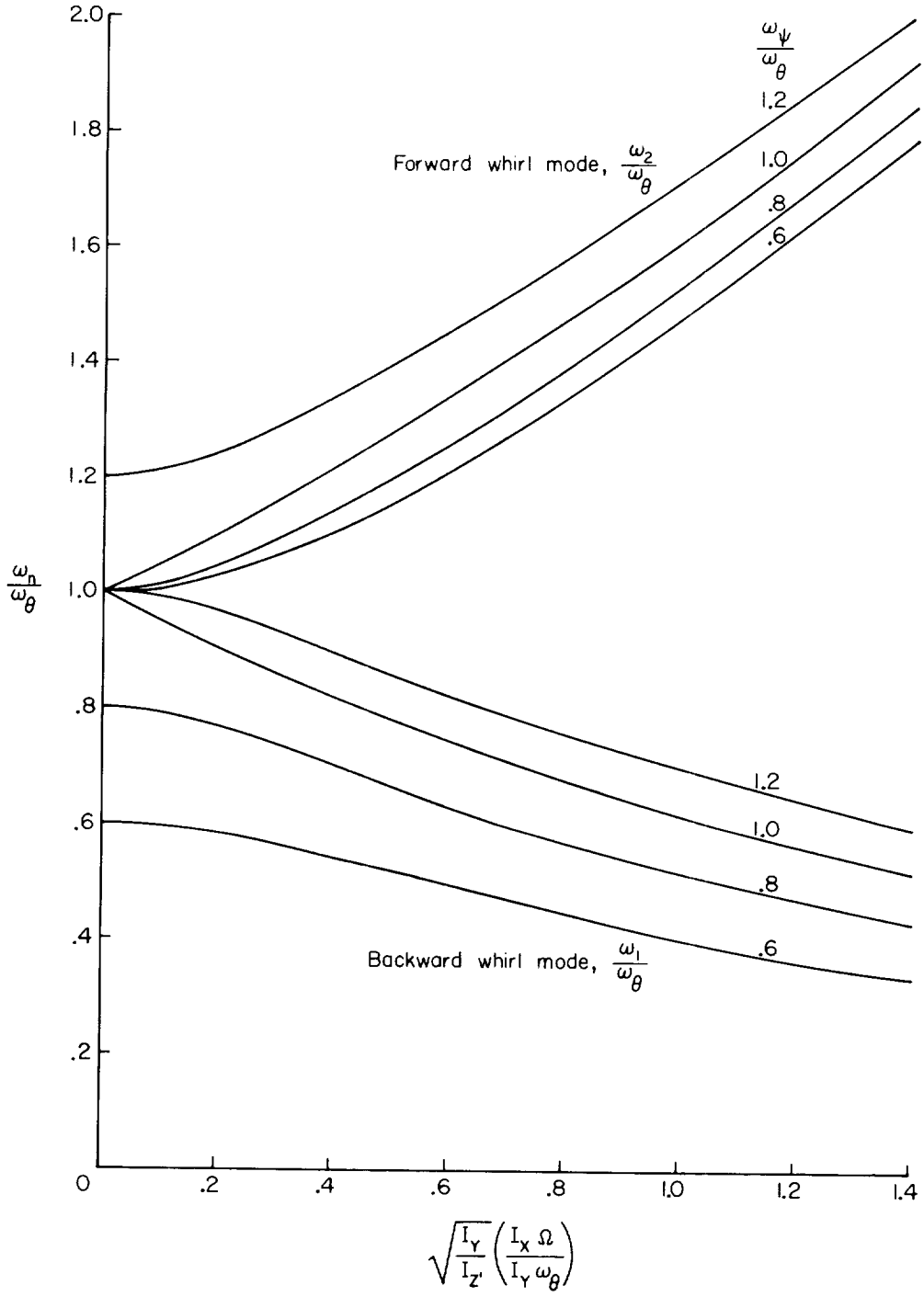

Figure 7.- Gyroscopic effect on whirl mode frequencies (plot of eq. (13c)).

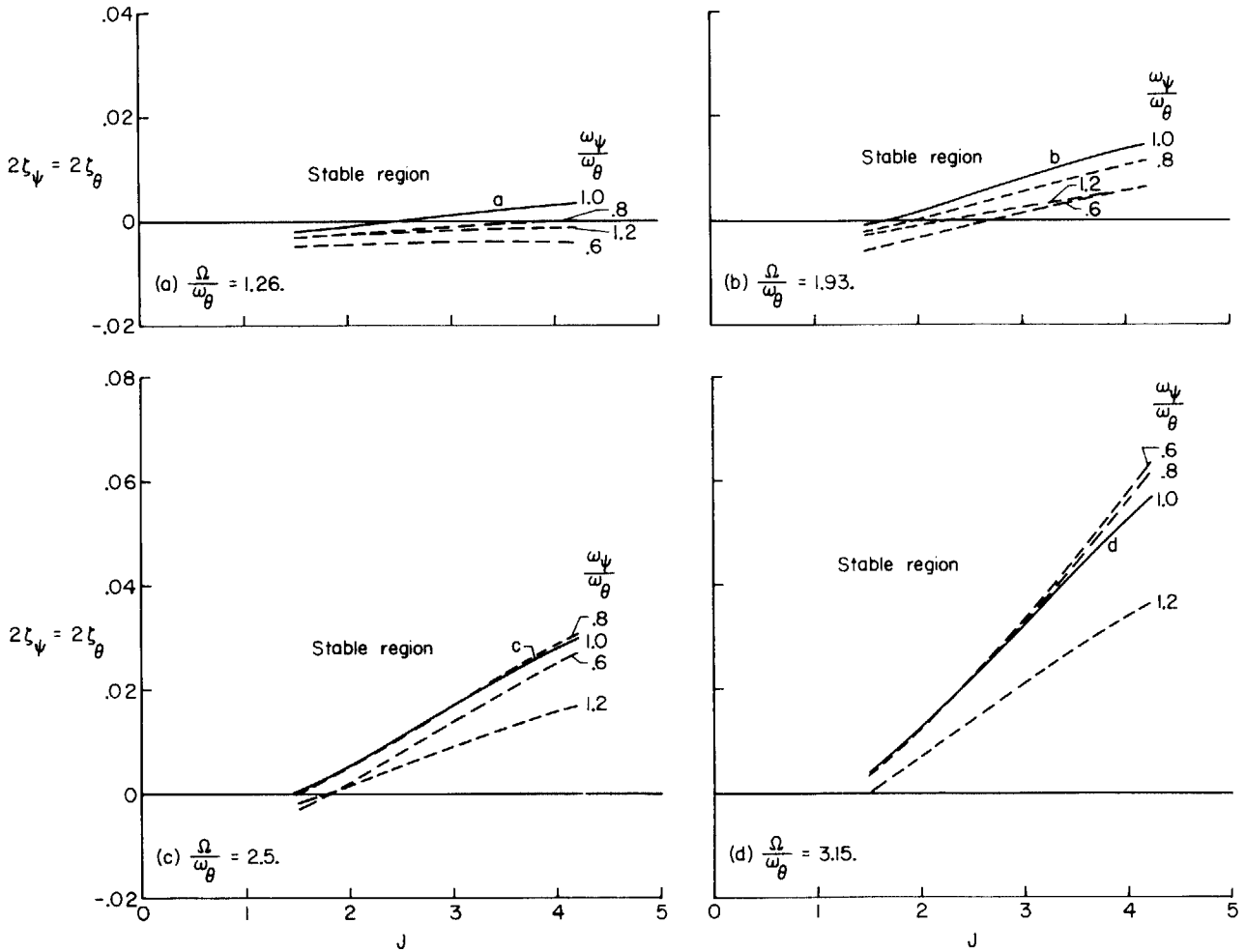

Figure 8.- Propeller whirl stability boundaries for propeller A over ranges of frequency ratio $\frac{\omega_\psi}{\omega_\theta}$ and $\frac{\Omega}{\omega_\theta}$. $T_c = 0$; $C_{Y_\theta} = 0$; $\frac{e_\psi}{e} = \frac{I_Z}{I_Y} = 1$; $\frac{1}{\mu} = 0.00978$; $\frac{I_X}{I_Y} = 0.1184$; $\frac{e}{D} = 0.235$.

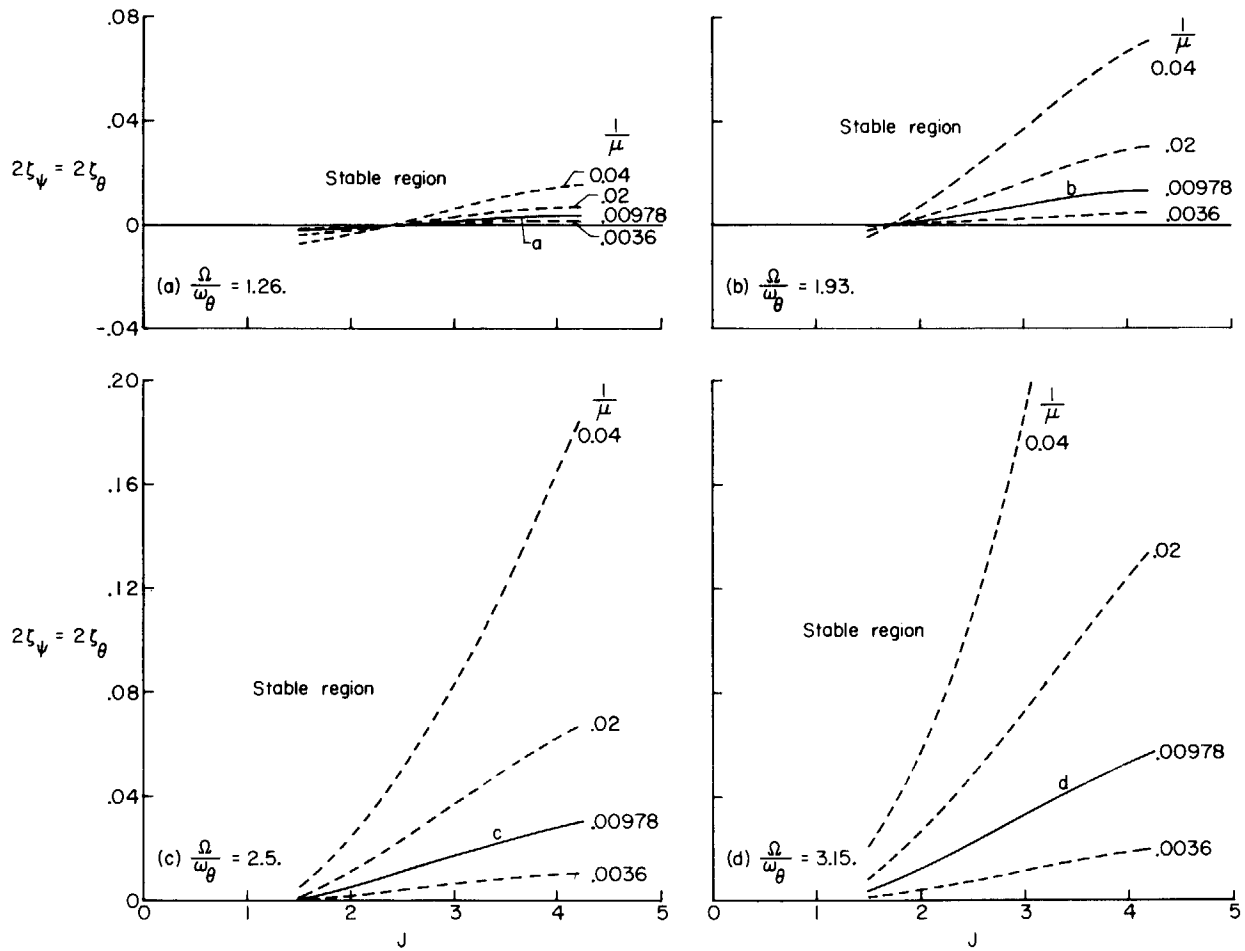

Figure 9.- Effect of inertia-density ratio $\frac{1}{\mu}$ on propeller whirl stability boundaries for propeller A with $T_c = 0$; $C_{Y_\theta} = 0$; $\frac{e_\psi}{e} = \frac{I_Z}{I_Y} = 1$; $\frac{\omega_\psi}{\omega_\theta} = 1.0$; $\frac{I_X}{I_Y} = 0.1184$; $\frac{e}{D} = 0.235$.

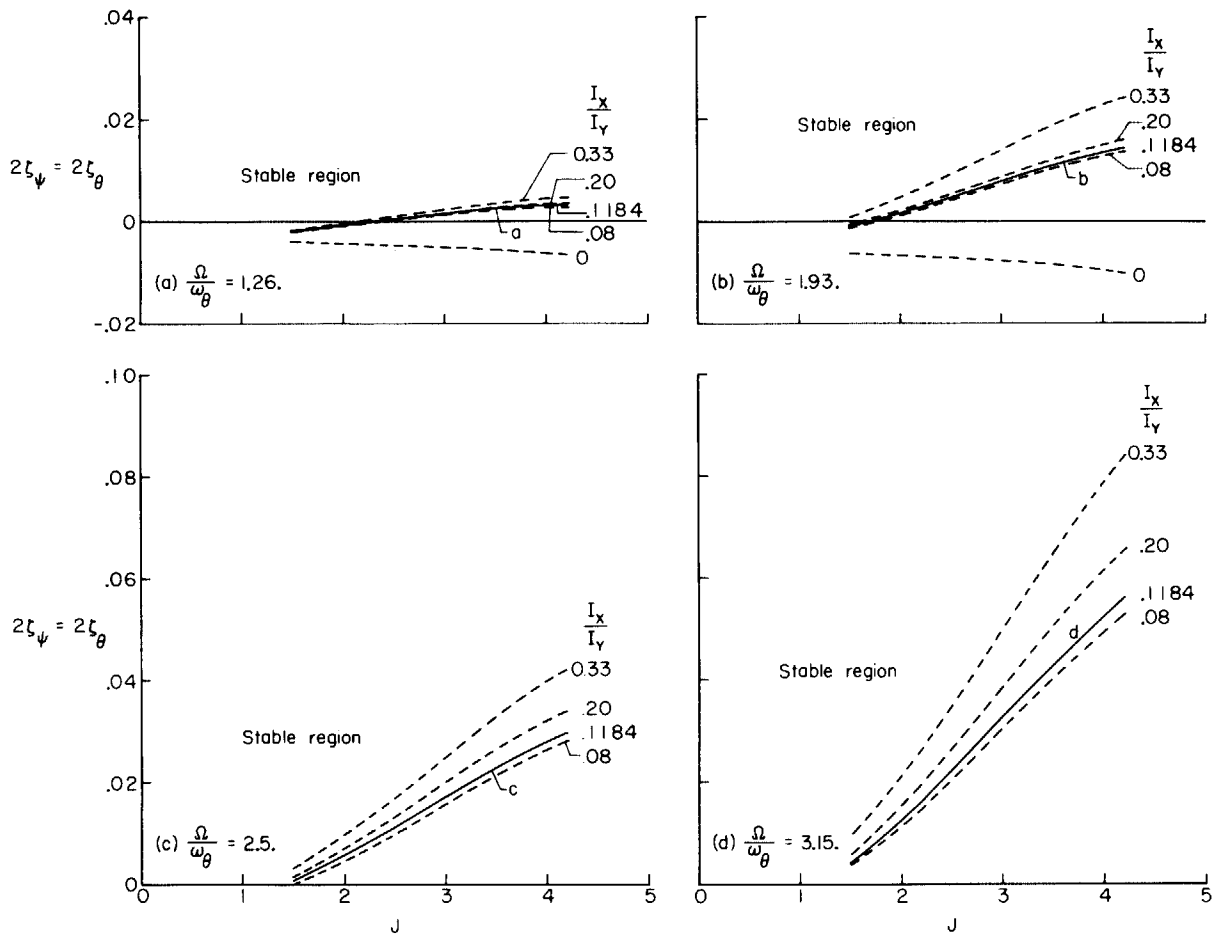

Figure 10.- Effect of inertia ratio $\frac{I_X}{I_Y}$ on propeller whirl stability boundaries for propeller A with $T_c = 0$; $C_{Y_\theta} = 0$; $\frac{e_\psi}{e} = \frac{I_Z}{I_Y} = 1$; $\frac{\omega_\psi}{\omega_\theta} = 1.0$; $\frac{1}{\mu} = 0.00978$; $\frac{e}{D} = 0.235$.

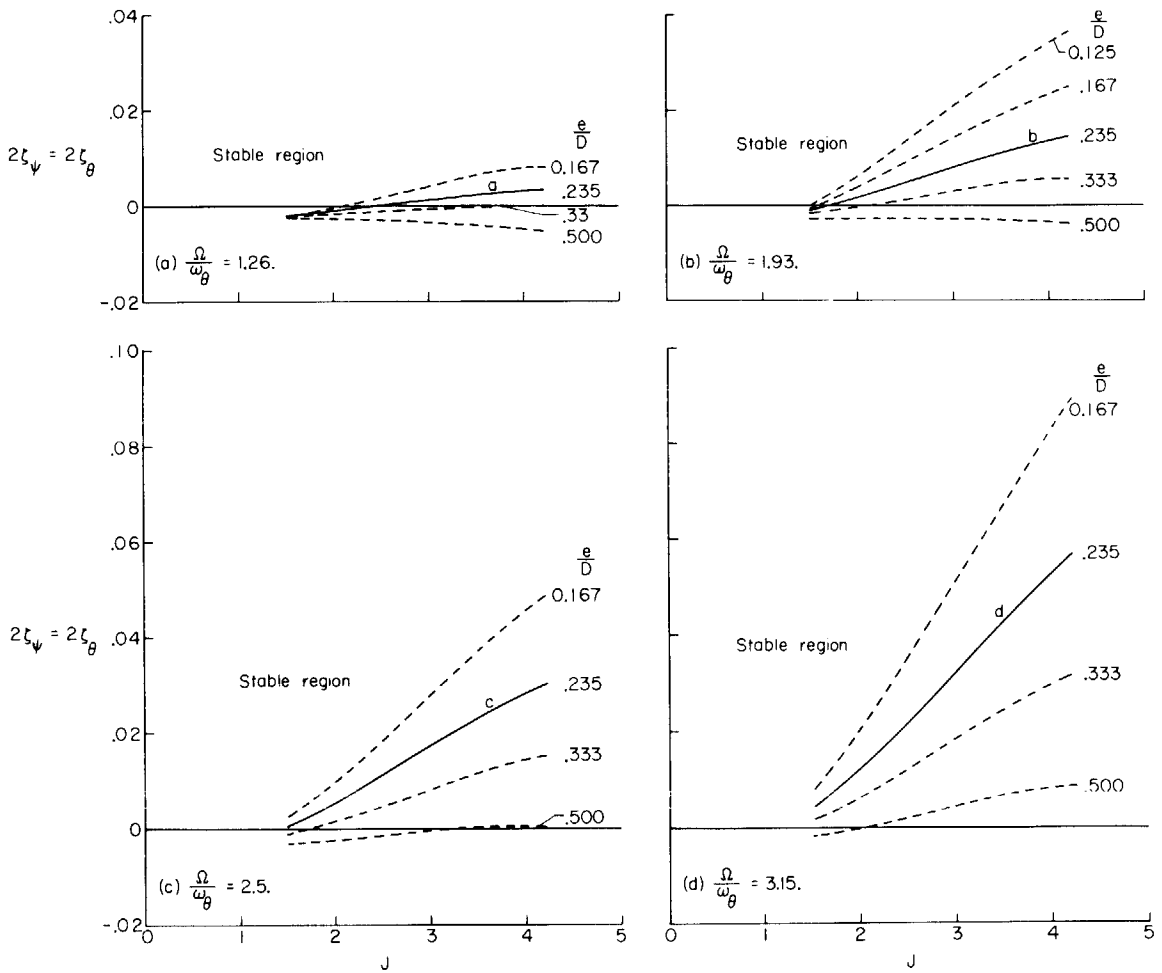

Figure 11.- Effect of $\frac{e}{D}$ on propeller whirl stability boundaries for propeller A with $T_c = 0$; $C_{Y_\theta} = 0$; $\frac{e_\psi}{e} = \frac{I_Z}{I_Y} = 1$; $\frac{\omega_\psi}{\omega_\theta} = 1.0$; $\frac{1}{\mu} = 0.00978$; $\frac{I_X}{I_Y} = 0.1184$.

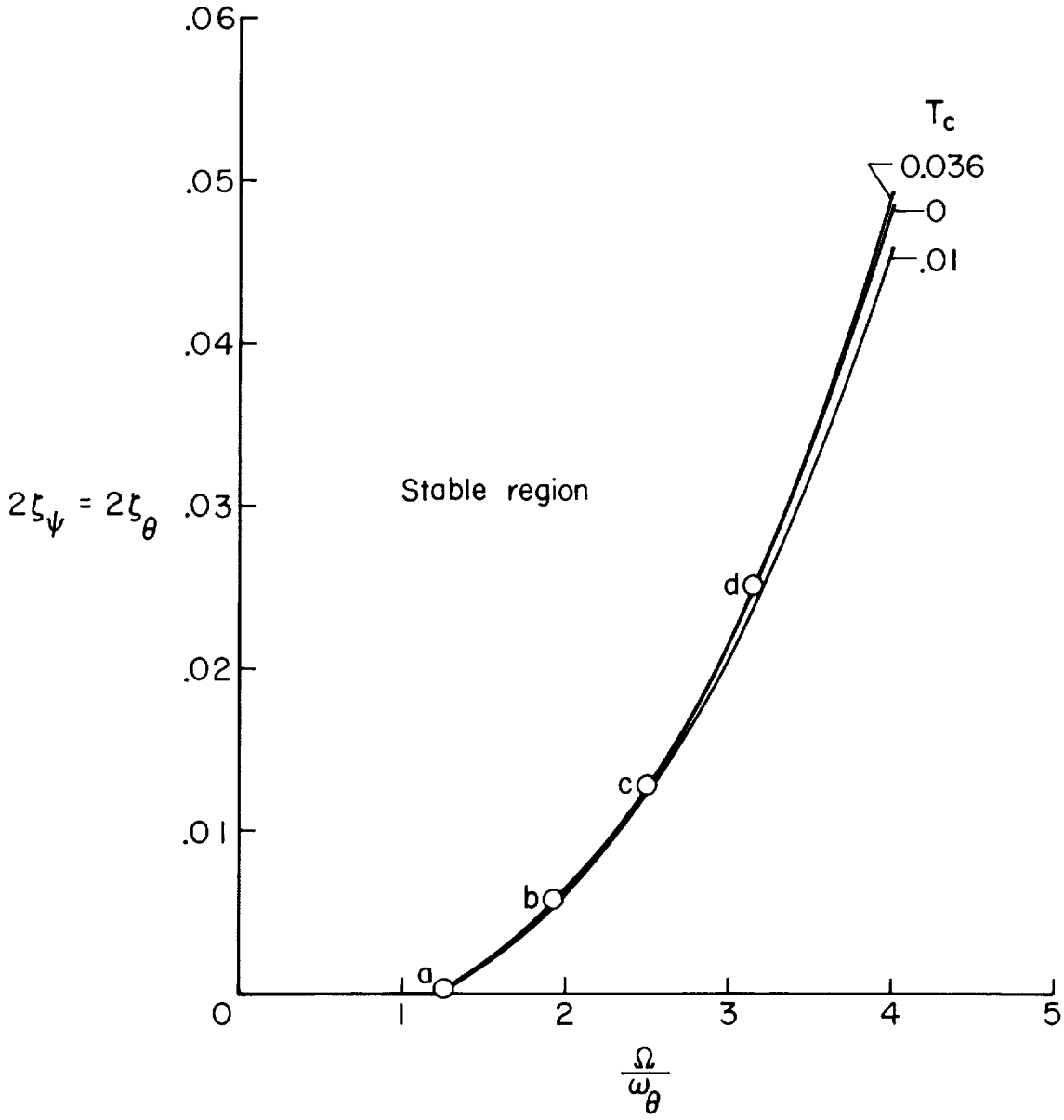

Figure 12.- Effect of thrust coefficient T_c on propeller whirl stability boundaries for propeller A with $J = 2.65$; $C_{Y_\theta} = 0$; $\frac{e_\psi}{e} = \frac{I_Z}{I_Y} = 1$; $\frac{\omega_\psi}{\omega_\theta} = 1.0$; $\frac{1}{\mu} = 0.00978$; $\frac{I_X}{I_Y} = 0.1184$; $\frac{e}{D} = 0.235$. Symbols correspond to solid-line reference curves in figure 8.

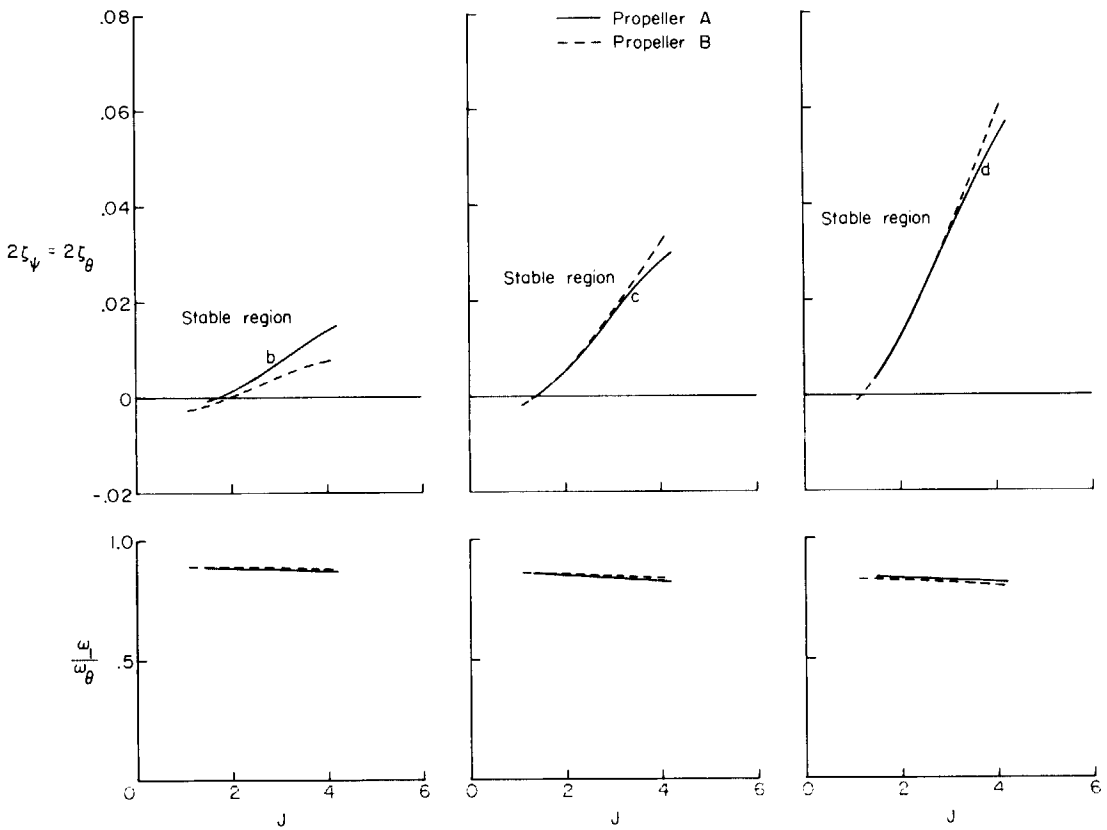

(a) $\frac{\Omega}{\omega_\theta} = 1.93.$ (b) $\frac{\Omega}{\omega_\theta} = 2.5.$ (c) $\frac{\Omega}{\omega_\theta} = 3.15.$

Figure 13.- Comparisons of propeller whirl stability boundaries for two different windmilling propellers ($T_c = 0$) with $C_{Y_\theta} = 0$; $\frac{e_\psi}{e} = \frac{I_Z}{I_Y} = 1$; $\frac{\omega_\psi}{\omega_\theta} = 1.0$; $\frac{1}{\mu} = 0.00978$; $\frac{I_X}{I_Y} = 0.1184$; $\frac{e}{D} = 0.235$.

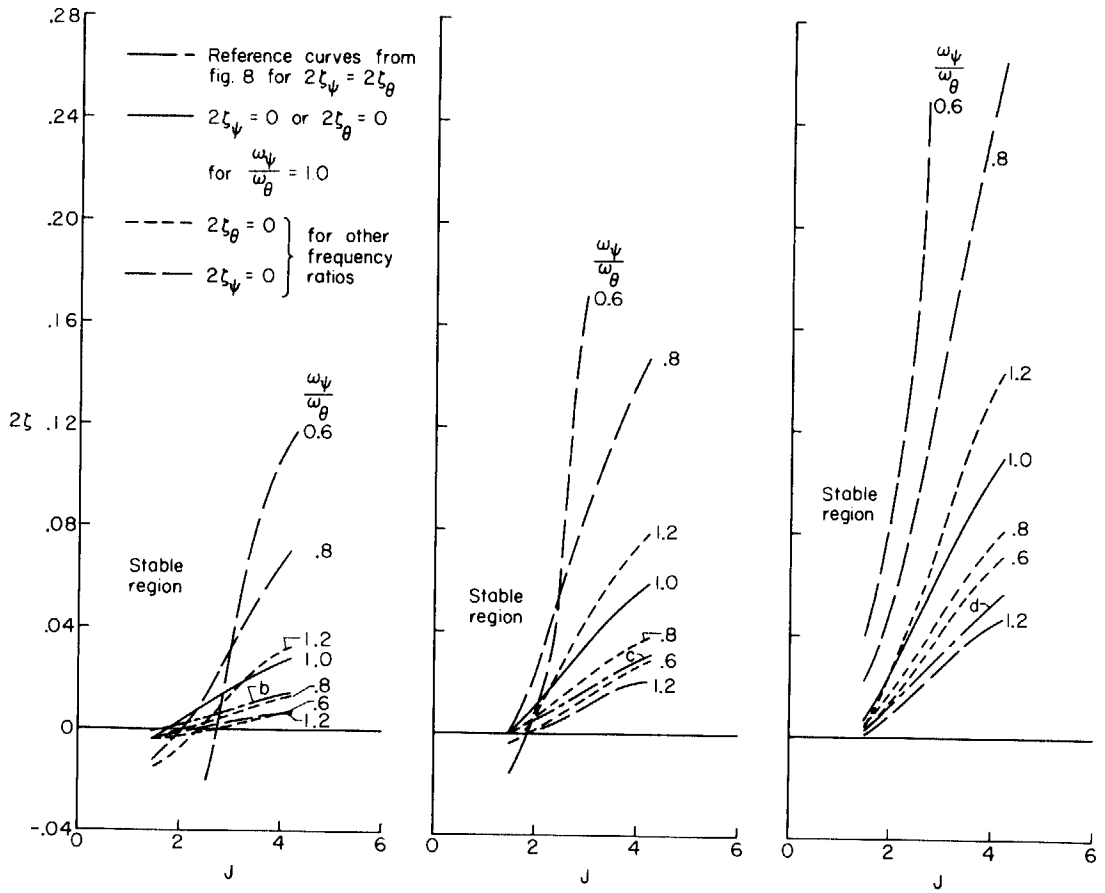

(a) $\frac{\Omega}{\omega_\theta} = 1.93.$ (b) $\frac{\Omega}{\omega_\theta} = 2.5.$ (c) $\frac{\Omega}{\omega_\theta} = 3.15.$

Figure 14.- Propeller whirl stability boundaries for propeller A for unsymmetrical damping with $T_c = 0$; $C_{Y_\theta} = 0$; $\frac{e_\psi}{e} = \frac{I_Z}{I_Y} = 1$; $\frac{1}{\mu} = 0.00978$; $\frac{I_X}{I_Y} = 0.1184$; $\frac{e}{D} = 0.235$.

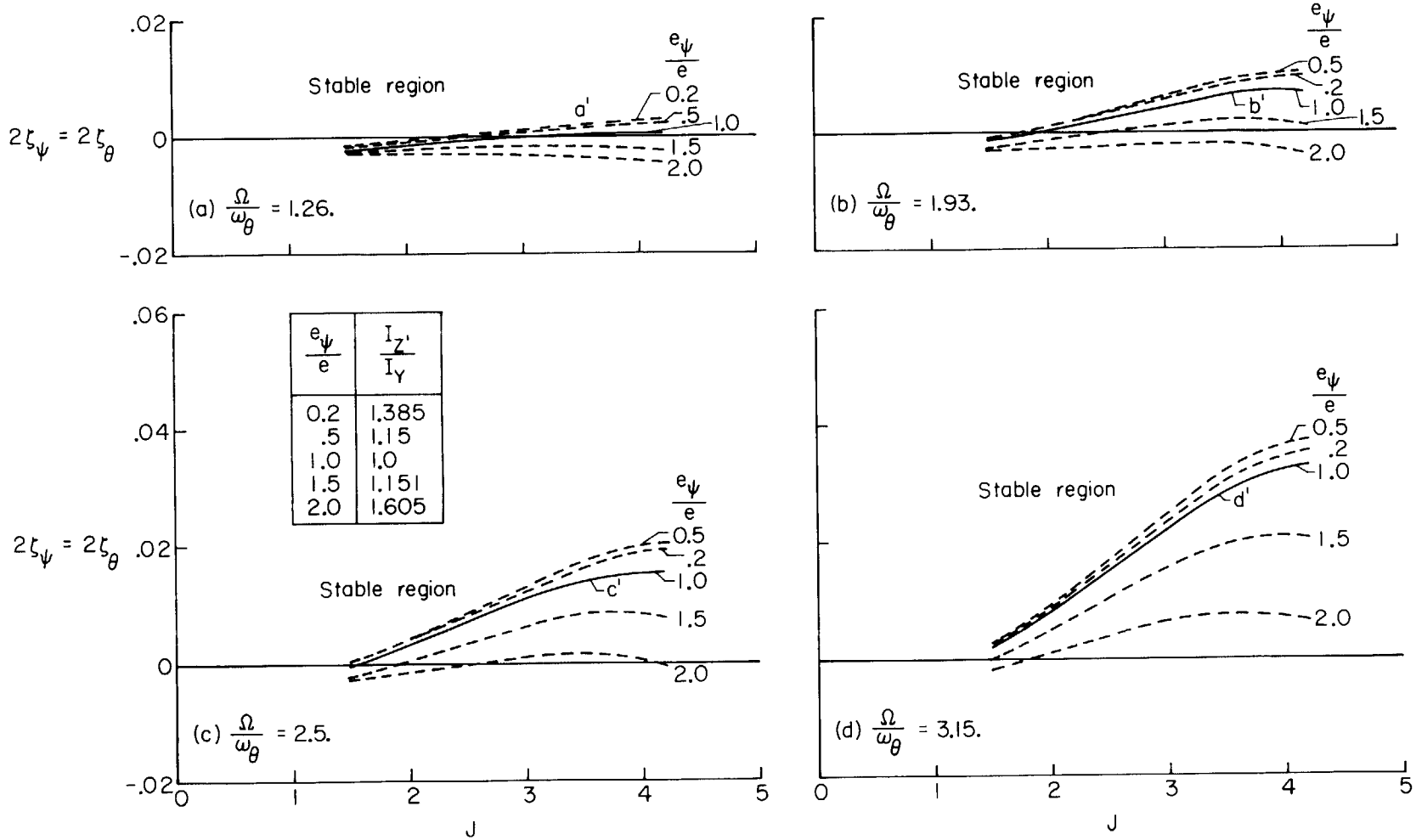

Figure 15.- Effect of different elastic centers in pitch and yaw on propeller whirl stability boundaries for propeller A with $T_c = 0$; $\frac{\omega_\psi}{\omega_\theta} = 1.0$; $\frac{1}{\mu} = 0.00978$; $\frac{I_X}{I_Y} = 0.1184$; $\frac{e}{D} = 0.235$.

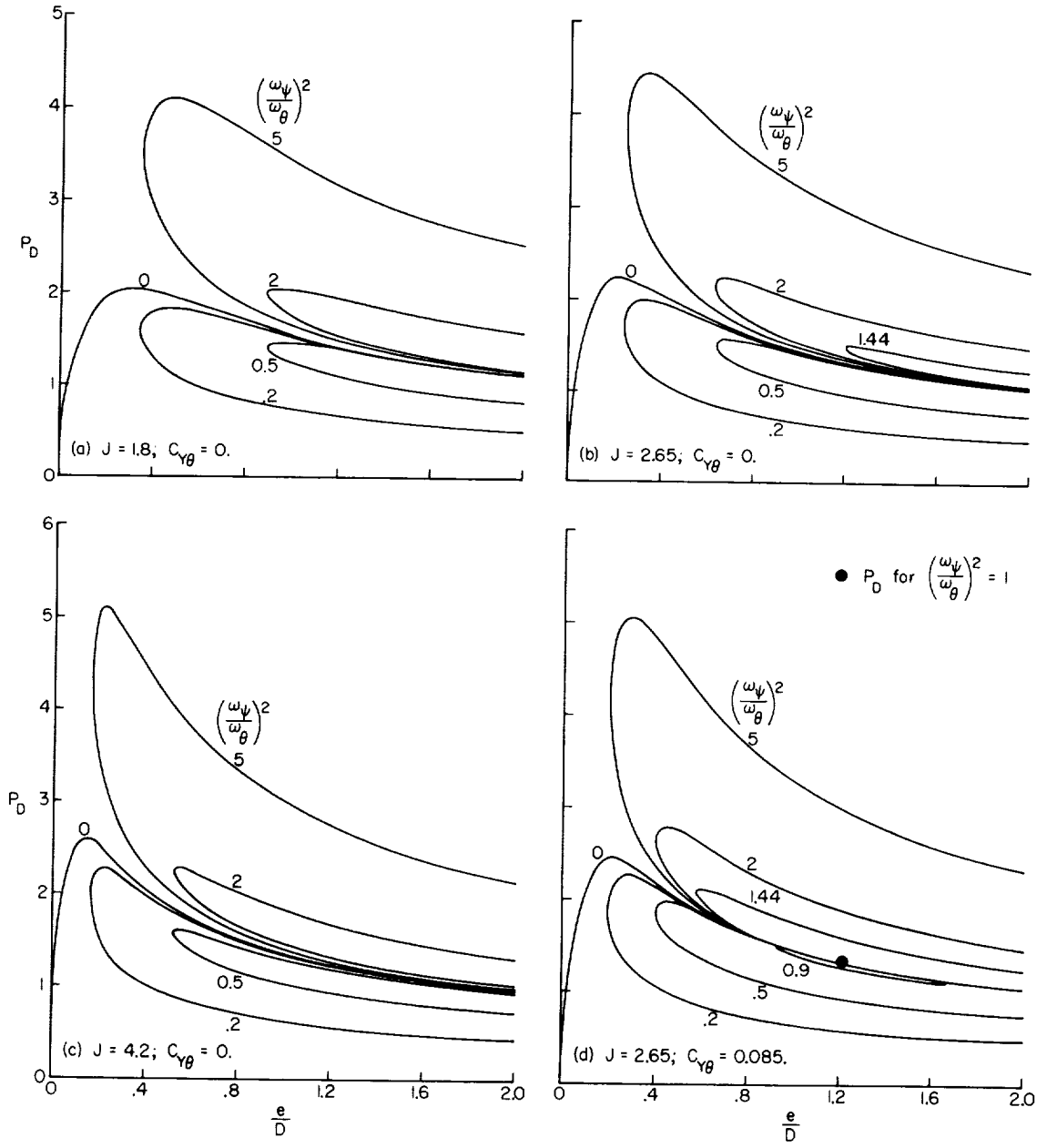

Figure 16.- Divergence boundaries for simplified engine-propeller combination based on propeller blade characteristics for propeller A with $T_c = 0$ and $\frac{e_\psi}{e} = \frac{I_Z}{I_Y} = 1$.

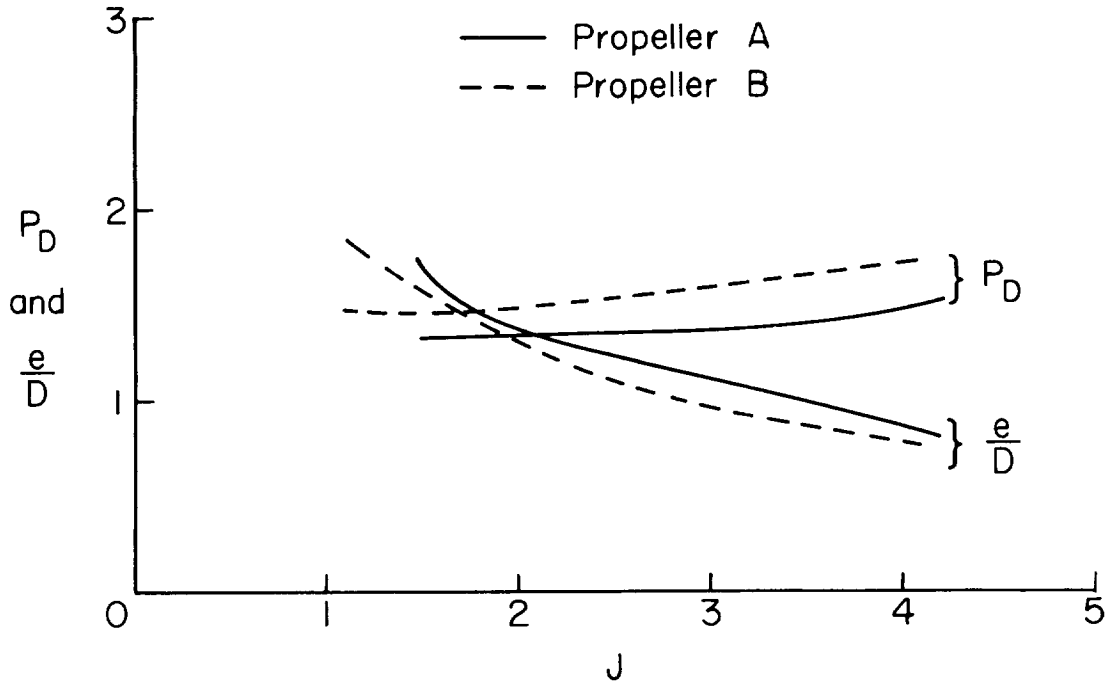

Figure 17.- Divergence boundaries for completely symmetrical system with a common elastic center (that is, $\frac{\omega_\psi}{\omega_\theta} = 1.0$ and $\frac{e_\psi}{e} = \frac{I_Z}{I_Y} = 1$; also $T_c = 0$).

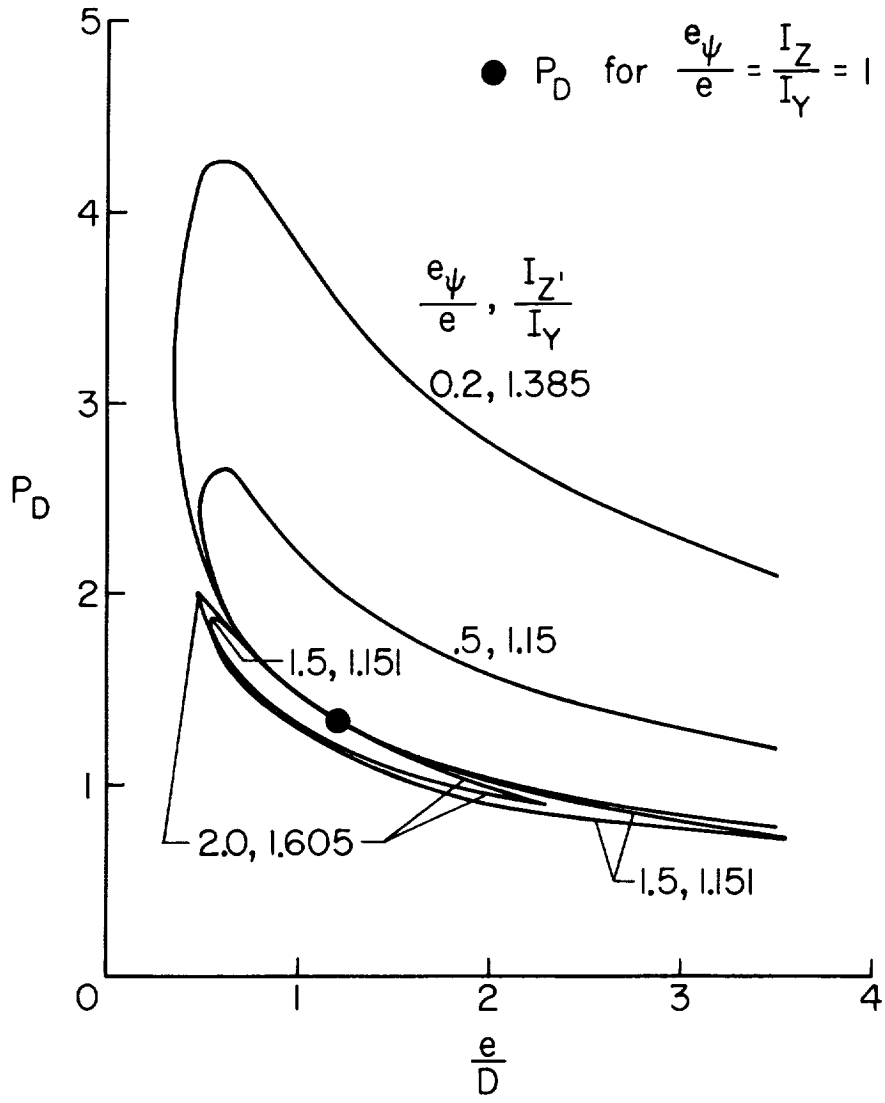

Figure 18.- Effect of different elastic centers in pitch and yaw on divergence boundaries of propeller A with $T_c = 0$; $J = 2.65$; $C_{Y_\theta} = 0.085$; $\frac{\omega_\psi}{\omega_\theta} = 1.0$.

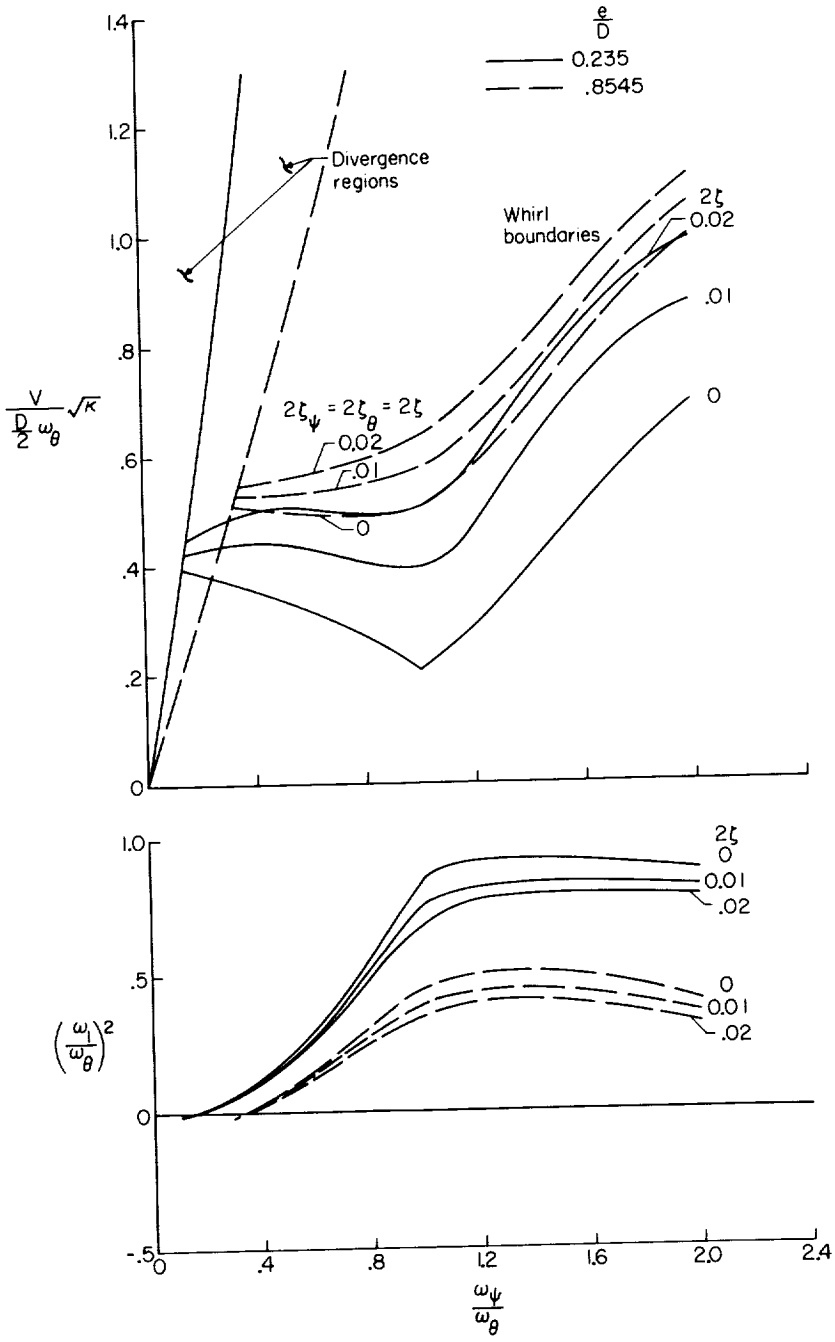

Figure 19.- Divergence and whirl boundaries for propeller A including the effect of damping for a wide range of frequency ratios with $T_c = 0$; $J = 2.65$; $C_{Y_\theta} = 0$; $\frac{e_\psi}{e} = \frac{I_Z}{I_Y} = 1$; $\frac{1}{\mu} = 0.00978$; $\frac{I_X}{I_Y} = 0.1184$.